Role Of Nucleoporins In Modulating Differentiation In Embryonal Carcinoma Cells

A Thesis

submitted to

Indian Institute of Science Education and Research Pune in partial fulfilment of the requirements for the BS-MS Dual Degree Programme

by

Jiffin Benjamin

Indian Institute of Science Education and Research Pune
Dr. Homi Bhabha Road,
Pashan, Pune 411008, INDIA.

April, 2020

Supervisor: Kundan Sengupta

CERTIFICATE

This is to certify that this dissertation entitled “Role Of Nucleoporins In Modulating Differentiation In Embryonal Carcinoma Cells” towards the partial fulfilment of the BS-MS dual degree programme at the Indian Institute of Science Education and Research, Pune represents study/work carried out by Jiffin Benjamin at Chromosome Biology Lab (CBL), IISER Pune under the supervision of Dr. Kundan Sengupta, Associate Professor, Department of Biology, IISER Pune during the academic year 2019-2020.

Student

Jiffin Benjamin
20151096
5th Year BS-MS
IISER Pune

Supervisor

Dr. Kundan Sengupta
Associate Professor
Department of Biology
IISER Pune

DECLARATION

I hereby declare that the matter embodied in the report entitled “Role Of Nucleoporins In Modulating Differentiation In Embryonal Carcinoma Cells” are the results of the work carried out by me at the Department of Biology, Indian Institute of Science Education and Research (IISER) Pune, under the supervision of Dr. Kundan Sengupta and the same has not been submitted elsewhere for any other degree.

Student

Jiffin Benjamin
20151096
5th Year BS-MS
IISER Pune

Supervisor

Dr. Kundan Sengupta
Associate Professor
Department of Biology
IISER Pune

ABSTRACT

NTERA-2 cl.D1 (NT2/D1) is an embryonal carcinoma cell line that differentiates into a neuronal phenotype upon induction with retinoic acid (RA). Cellular differentiation incorporates various stimuli and involves multiple layers of regulation in determining cell fate. In NT2/D1 cells, the nucleoporin Nup93, regulates the expression of the HOXA gene cluster during differentiation. Nucleoporins are channel proteins embedded in the nuclear envelope and are canonically involved in nucleocytoplasmic transport of RNA and proteins. However, recent studies implicate their roles in gene regulation and cell fate determination. Here we investigated the role of the Nup93-subcomplex proteins - Nup93, Nup188 and Nup205 in differentiation. We show that Nup93 subcomplex proteins regulate the expression of pluripotency and lineage genes. Furthermore, induction of differentiation upon RA treatment reveals a differential role of Nup93 and Nup188 on differentiation. Here we show a novel role for Nup205 in the formation of cell aggregates in embryonal carcinoma cells. We also showed that RA treatment in NT2/D1 differentially altered lamin protein levels, and examined lamin function during differentiation. In addition, preliminary data substantiates the contribution of mechanosignaling in differentiation. Taken together our data reveals a regulatory role for the Nup93 subcomplex in modulating neuronal differentiation in NT2/D1 cells.

INDEX

LIST OF FIGURES AND TABLES

ACKNOWLEDGEMENTS

I would like to thank Dr. Kundan Sengupta, Chromosome Biology Lab, Indian Institute of Science Education and Research, Pune, for giving me an opportunity to work in his lab. I extend my gratitude for his valuable inputs, support and encouragement throughout the project. I would like to thank Dr. Ajay Labade and Adwait Salvi for their invaluable mentorship towards the start of the project, without which this work would not have taken off. I am grateful to all the CBL lab members for their constant support, review and guidance even in the littlest of things, which helped contribute towards thorough project work.

I would like to thank Dr. Krishanpal Karmodiya, IISER Pune and Dr. Jomon Joseph, NCCS Pune for their valuable inputs. I thank Dr. Aurnab Ghose and microscopy facility, IISER Pune, for providing a facility for imaging. I would also like to express my gratitude to all my friends and family for their constant support throughout the journey. Lastly, I would like to thank IISER Pune for providing such an opportunity and a wonderful facility for pursuing research.

INTRODUCTION

It is well established that loss of contact inhibition and apoptosis is a hallmark of cancers. Cancer cells gain increased metastatic potential and vascularisation, that promotes tumor growth. Due to the heterogeneous nature of cancer cells, cancers can initiate from the activation of various pathways. Teratocarcinoma is a form of testicular germ cell tumor that is highly malignant. This tumor has undifferentiated cells referred to as embryonal carcinoma (EC), due to its resemblance with embryonic stem cells, capable of differentiating into the three different germ layers. Due to the presence of the EC component in teratocarcinomas, the tumor tissue recapitulates events during early development and is considered as a candidate model to study cellular differentiation (Przyborski et al., 2004; Skotheim et al., 2005). NTERA-2 cl.D1 (NT2/D1) is one such embryonal carcinoma derived from a human lung metastasis of a germ cell tumor. NT2/D1 has been extensively used as a model for cellular differentiation as they can be terminally differentiated using external inducers. Adding BMP7 (Bone Morphogenetic Protein-7) shows an epithelial phenotype (Andrews et al., 1994; Caricasole et al., 2000), whereas RA (Retinoic Acid) treatment induces a neuronal phenotype (Andrews, 1984; Pierce et al., 1999); (Coyle et al., 2011). These cells are functional neurons, since these differentiated cells when transplanted into rodent brains, survived for over a year, improving conditions of motor function in animal models that recapitulate stroke-like conditions (Nelson et al., 2002).

Retinoic Acid (RA) is a Vitamin A-derived morphogen that plays a major role in embryonic development. RA binds to receptors within the nucleus from the retinoid receptor family, namely retinoic acid receptors (RARs), which is a transcription factor. RARs, along with retinoid X receptors (RXRs), forms a heterodimer upon ligand binding and targets retinoic acid response elements (RAREs) present in the promoter regions of genes, initiating transcription. RXRs can also form heterodimers with receptors of other families such as PPAR, LXR, and FXR, and hence the binding of RA on RARs can upregulate genes like HOXA1 while competitively suppress the transcription of others like TRX1 and BSEP (Kam et al., 2012). In early

mouse spinal neurogenesis, RA is directly involved in upregulating the proneural gene Neurogenin2 (Neurog2) through an enhancer element that contains two RARE domains (Ribes et al., 2008). RA-mediated neuronal differentiation of NT2/D1 cells has been extensively characterised (Coyle et al., 2011). Retinoic acid addition leads to the spatio-temporal regulation of HOX gene expression (Boncinelli et al., 1991).

The HOX homeobox genes encode transcription factors essential for embryonic development (Taylor, 2000). The HOX gene cluster is collinear in organization and expression, which is conserved in evolution (Dressler and Gruss, 1989; Duboule, 2007). In NT2/D1 cells, RA-mediated neuronal differentiation activates HOXA genes in a temporal manner during differentiation, with CTCF as a potential regulator of gene expression (Xu et al., 2014). Nucleoporin Nup93 that interacts with Nup188 and Nup205 forming the Nup93-subcomplex, is involved in nucleo-cytoplasmic transport. Furthermore, the Nup93 sub-complex is enriched on the promoters of HOXA1, HOXA3, and HOXA5 and represses their expression (Labade et al., 2016).

Nuclear pore complexes (NPCs) are channel proteins embedded in the nuclear envelope and are essential for nucleocytoplasmic transport, however, their non-canonical functions include transcriptional regulation (Capelson et al., 2010; Casolari et al., 2004), DNA damage repair (Nagai et al., 2008), cell fate determination (D'Angelo et al., 2012; Ibarra et al., 2016) and genome organisation (Schermelleh et al., 2008). Although NPCs are embedded in the nuclear membrane, certain nucleoporins leave the NPC and have off-pore functions. Nup98 and Nup50, for example, localise in the nucleoplasm, where its dynamic movement is dependent on RNA polymerase I and II mediated transcriptional activity (Buchwalter et al., 2014; Griffis et al., 2002). Nuclear GM1 ganglioside regulates neurogenic gene expression and colocalizes with NPCs at the nuclear periphery in differentiated neurons (Tsai et al., 2016). Nup93 regulates HOXA gene expression in a spatiotemporal manner in NT2/D1 cells (Labade et al., 2019). Here we investigated the role of the Nup93 sub-complex (Nup188-Nup93-Nup205) in Retinoic Acid (RA)-mediated differentiation of NT2/D1 cells.

In addition to nucleoporins, the nuclear envelope is composed of lamins that interact with nucleoporins. Lamins are type V intermediate filaments that constitute the nuclear lamina and provide structural support to the nucleus. Lamins are of two types A-type lamins and B-type lamins. Lamin A/C is involved in genome organisation, tethering heterochromatin and regulates differentiation (Solovei et al., 2013). During early brain development, lamin B1 regulates the differentiation of murine neural stem cells (NSCs) into neurons (Mahajani et al., 2017). Generally, lamin A levels are lower in undifferentiated cell types and are relatively higher in differentiated cells (Zuo et al., 2012). A notable exception to this are neurons, where differentiation into neuronal lineage from a pluripotent state lowers lamin A levels. Heterogeneity in the expression levels of the different lamin subtypes was seen in the neural cells of the adult rat cerebral cortex, with reduced lamin A in neurons (Takamori et al., 2018). Taken together these evidence suggest mutually exclusive roles of lamins in neuronal differentiation. Furthermore, the lamin A/C promoter contains a RARE binding site that is transcriptionally activated upon RA treatment in the EC cell line P19 (Okumura et al., 2000). This is in contrast to RA-mediated neuronal differentiation in NT2/D1 cells, where lamin A/C levels decrease upon RA treatment (Pierce et al., 1999). Lower lamin A levels correlate with tissue stiffness, suggesting that mechanical cues impact lamin A transcription. Further studies showed that the effect of RA on LMNA expression was suppressed on softer matrices (Swift et al., 2013). Mechanosignaling drives cellular differentiation, with softer matrix stiffness being neurogenic, while stiffer matrices promote osteogenesis (Engler et al., 2006). The scaling of lamin A with tissue stiffness makes lamins interesting proteins in the context of neuronal differentiation. We, therefore, examined the function of lamins in the context of matrix stiffness, in modulating RA-mediated differentiation of NT2/D1 cells.

RESULTS

Characterisation of differentiation in NT2/D1 embryonal carcinoma cells

NT2/D1 cells differentiate into the neuronal lineage upon retinoic acid (RA) treatment. This is followed by morphological changes to a more neuronal phenotype. The cells initially show a more epithelial-like morphology at higher confluency and a more elongated phenotype at lower confluency (Fig. 1C). RA treatment induces cell flattening, elongation and branching, characteristic of differentiation into a neuronal cell type. Levels of the pluripotency markers Oct4, Sox2 and Nanog showed a collective decrease in their transcript levels over an 8 day differentiation period (Fig. 1D). Oct4 and Nanog levels were undetectable by Day 8 of RA treatment, with Nanog showing a decrease from Day 2 onwards. Sox2 levels fluctuate across the days but show a marginal decrease in their expression levels by Day 8 (Fig. 1D). This correlates with the role of Sox2 in neurogenesis since Sox2 is an established marker of neural progenitor cells (Bowles et al., 2019; Ferri et al., 2004). The overall trend in the expression levels of these genes supports the notion that NT2/D1 cells transition from a pluripotent state to a more differentiated neuronal cell fate. We, therefore, tested the levels of markers that represent the three individual germ layers, namely endothelial (VEGFR), mesodermal (Mesp2) and ectodermal - neural lineage (Pax6) (Fig. 1E-G). VEGFR levels decline (by ~70%) from Day 2 and do not show an increase through the time course of differentiation. In contrast, Mesp2 decreases (~50%) on Day 2, but recovers from Day 4, with the levels remaining relatively lower (by ~30%) than basal levels on Day 8. Pax6 levels increase significantly on Day 2 to ~170 folds and increase further on Day 4 to ~600 folds. Taken together, the collective levels of these transcripts are characteristic of differentiation into the neuronal lineage.

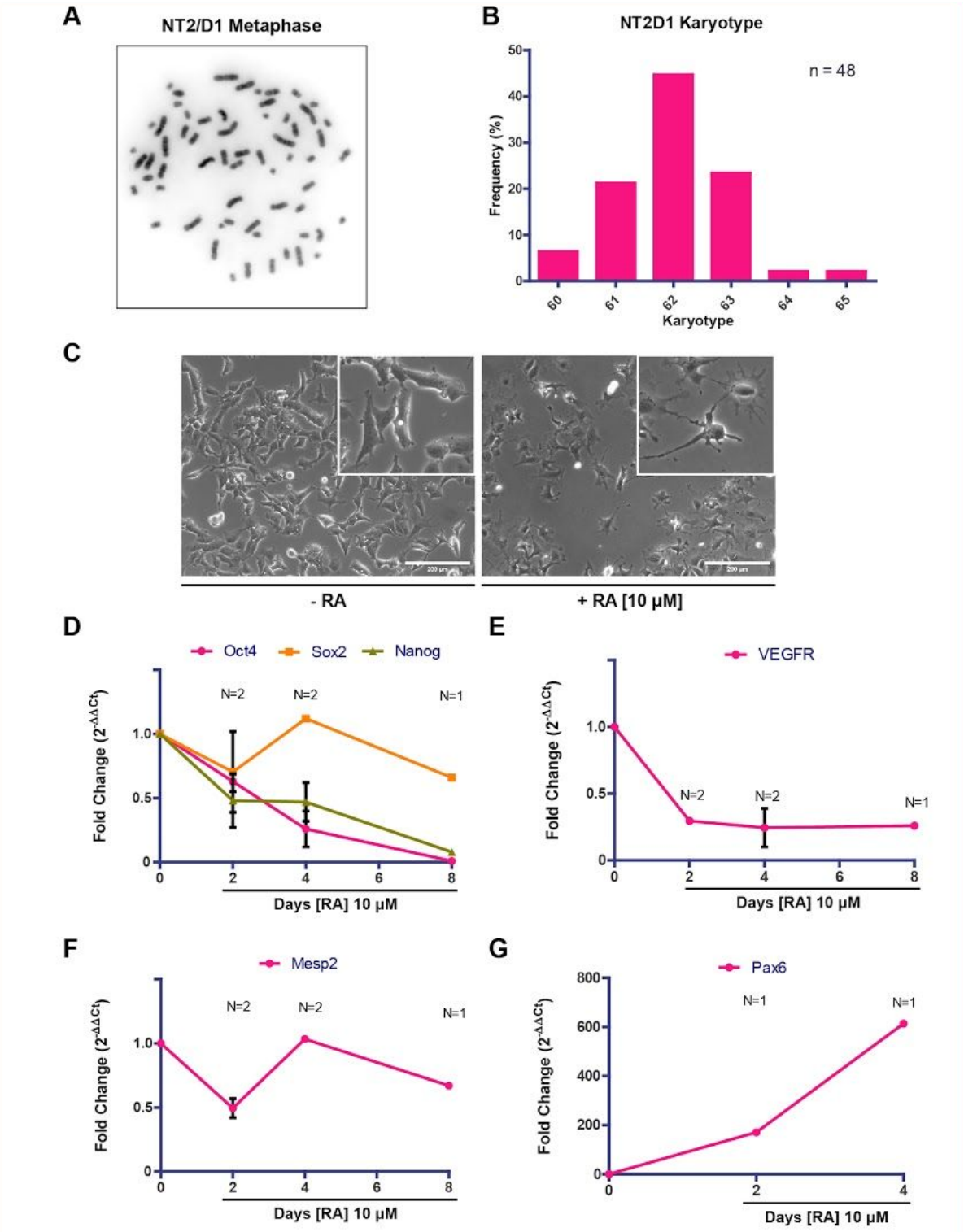

Fig. 1: Characterisation of neuronal differentiation in NT2/D1. (A) Representative image of a metaphase spread of NT2/D1 cells. (B) Quantification of the modal number across n=48 spreads. (C) Morphology of the cells under various conditions as mentioned. Scale bar = 200 µm. (D) Expression levels of Oct4, Sox2 and Nanog across day 0, 2, 4 and 8 with RA treatment. Biological replicates as mentioned. Error bars represent SEM. (E) VEGFR, (F) Mesp2 and (G) Pax6 levels upon RA treatment on days 0, 2, 4 and 8. Biological replicates as mentioned. Error bars represent SEM.

Effect of nucleoporin knockdown on NT2/D1 differentiation

Nucleoporins are canonically involved in nucleocytoplasmic transport. However, in addition, nucleoporins are also involved in gene regulation and cell fate determination (Capelson et al., 2010; Casolari et al., 2004), (D'Angelo et al., 2012; Ibarra et al., 2016)). Expression of the developmentally important HOXA gene cluster is controlled by Nup93 during neuronal differentiation in NT2/D1 (Labade et al., 2019). In this context, to assess the role of nucleoporins on neuronal differentiation, RA treatment was performed on cells in the background of Nup188, Nup93 and Nup205 knockdown in NT2/D1 cells, followed by an assessment of the transcript levels of pluripotency and lineage markers across an 8-day regimen of RA treatment (Fig. 2-4). Cells were pulsed with siRNA at intervals of every 3 days, while RA was added once every 2 days (Fig. 2A). Overall, the expression levels of the three nucleoporins Nup93, Nup188, and Nup205 remained relatively unaffected by the knockdown of one another, irrespective of RA treatment (Fig. 2B-D). The few deviations are: 1. Nup188 knockdown: levels of Nup93 and Nup205 decrease (~30% and ~25%, respectively) by day 10 in the presence of RA (Fig. 2B). 2. Nup93 knockdown: levels of Nup188 decrease in the presence and absence of RA (~20% and ~30%, respectively), while levels of Nup205 decrease (~20%) in the absence of RA, by day 4 (Fig. 2C).

Furthermore, RA treatment shows a striking decrease in Oct4 (~99%) and Nanog levels (~90%) by day 10, while Sox2 levels decreased by ~50% (Fig. 3A). Nup188 knockdown did not show an effect on RA induced gene expression (Fig. 3A). In the absence of RA, Nup188 knockdown upregulates Oct4, Sox2 and Nanog, whose levels peak at day 6, and returns back to basal levels by day 10. In all the three nucleoporin knockdowns, Sox2 levels increase on day 2 (~60%, ~130% and ~120% respectively for Nup188, Nup93 and Nup205 knockdown) and decrease to basal levels by day 4 (Fig. 3). Both Nup93 and Nup205 knockdowns upregulate Oct4 (~70% and ~100% respectively) by day 4, with and without RA treatment. In Nup205 knockdown, Nanog levels increased by day 4 (~100% and ~440% in the presence and absence of RA, respectively)(Fig. 3C).

In the presence of RA, transcript levels of VEGFR - an endothelial marker decreased by day 4 (~80%) and remained at a comparable level upto day 10. This was, however, unaffected by Nup188 knockdown (Fig. 4A). Similarly, in the presence of RA, Mesp2 levels fluctuate and remain slightly lowered (~30%) by day 10. Also, Pax6 levels peak by day 4 with RA treatment (~60 to ~350 folds across the knockdowns). Overall, the extent of increase in Pax6 levels are lower upon the depletion of the Nup93 sub-complex genes compared to RA treated cells alone (Fig. 4). In the absence of RA, Nup188 knockdown shows an increase in the levels of VEGFR and Mesp2 by day 4 (~80% and ~30%) and day 6 (~40% and ~60%) respectively, which returns to basal levels by day 8. Upon both Nup93 knockdown and RA treatment, VEGFR decreases by ~30%, as opposed to a ~70% decrease with RA treatment alone (Fig. 4B). Mesp2 levels go down upon both Nup93 and Nup205 knockdown (~70% decrease) by day 2 and are maintained upon RA treatment. WIthout RA, Mesp2 levels increase by day 4.

It is interesting to note that Pax6 levels showed a >100% increase upon Nup93 and Nup205 knockdown by day 2. In Nup205 knockdown by day 4, Pax6 levels return to basal levels without RA treatment, while showing a ~100% increase in VEGFR levels. Overall, Nup93 and Nup205 show similar trends in the expression of the 3 pluripotency markers (Oct4, Sox2, Nanog) and the 3 lineage markers (VEGFR, Mesp2, Pax6), both in the presence and absence of RA.

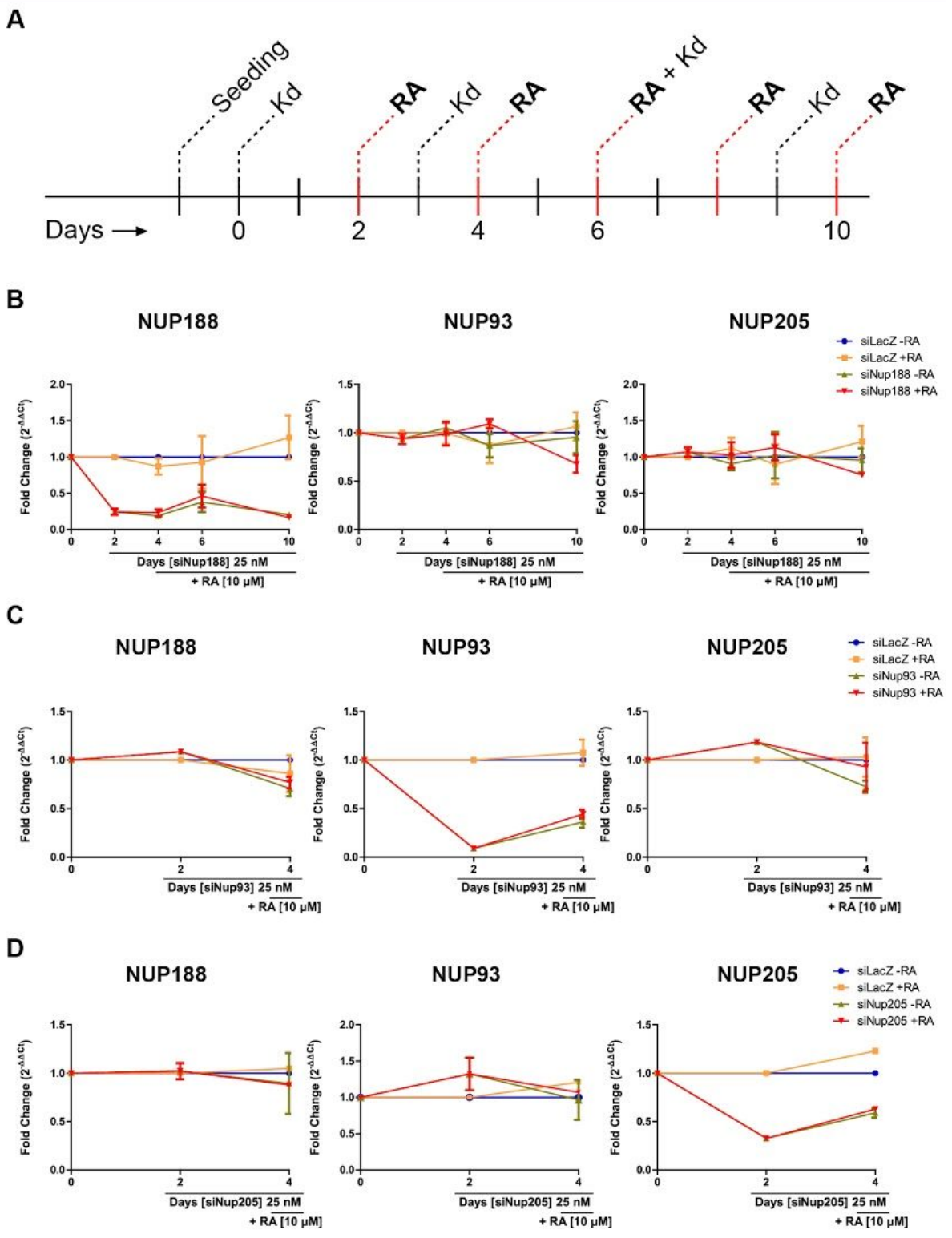

Fig. 2: Effect of the different knockdowns on nucleoporin gene expressions. (A) Scheme showing timeline of the knockdowns and RA treatment. (B-D) Transcript levels of Nup188, Nup93 and Nup205 upon: (A) Nup188 knockdown. Data for day 0 to day 6 from N=3, n=9 replicates and day 8 from N=2, n=6 replicates. (B) Nup93 knockdown. Data from N=2, n=6 replicates and (C) Nup205 knockdown. Data for Day 2 from N=3, n=9 replicates, day 4, -RA from N=2, n=6 and day 4, +RA from N=1, n=3 replicates. Error bars represent SEM.

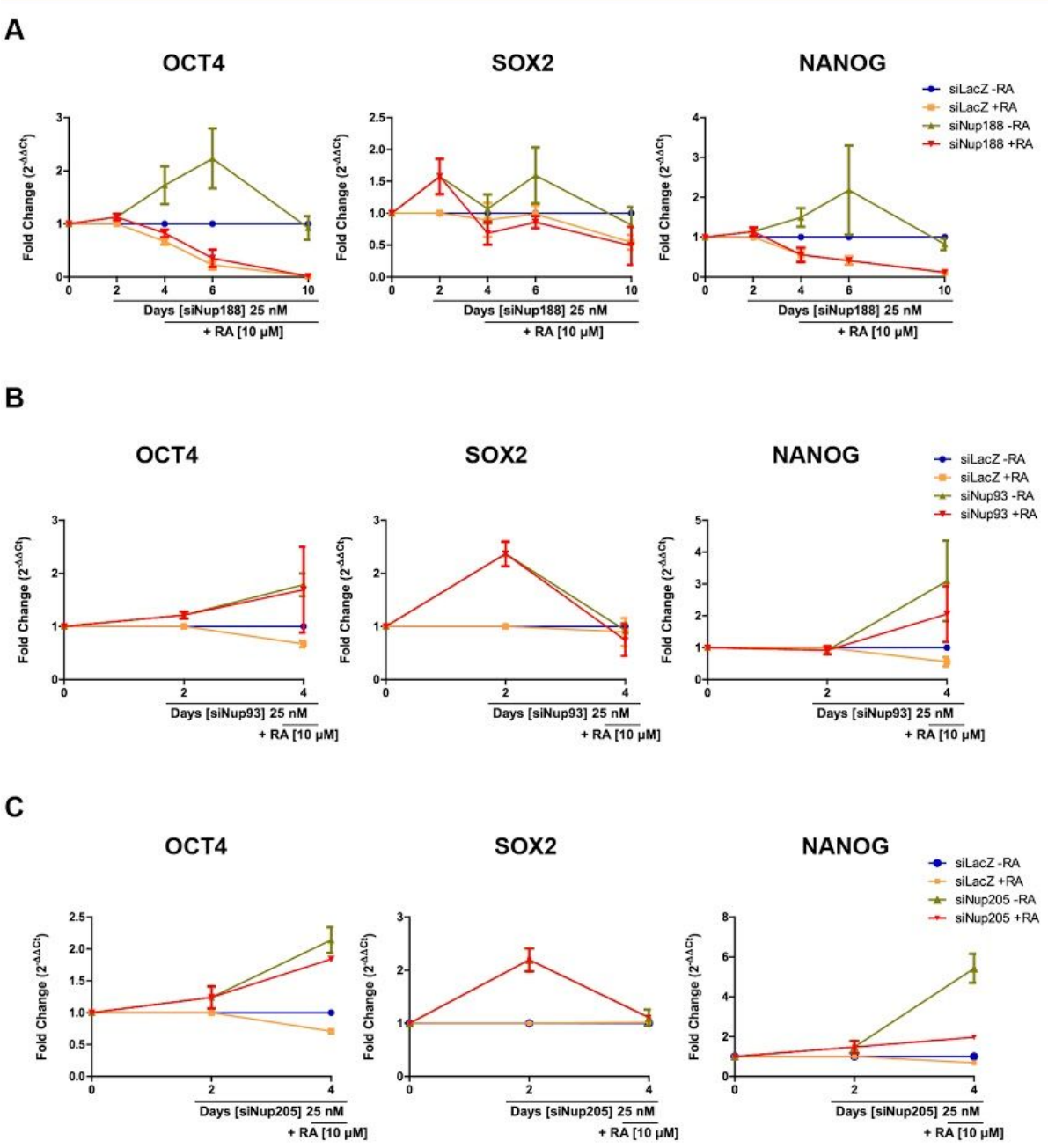

Fig. 3: Effect of the different knockdowns on OCT4, SOX2, NANOG gene expressions. Transcript levels of Oct4, Sox2 and Nanog upon: (A) Nup188 knockdown. Data for day 0 to day 6 from N=3, n=9 replicates and day 8 from N=2, n=6 replicates. (B) Nup93 knockdown. Data from N=2, n=6 replicates and (C) Nup205 knockdown. Data for Day 2 from N=3, n=9 replicates, day 4, -RA from N=3, n=9 and day 4, +RA from N=1, n=3 replicates. Error bars represent SEM.

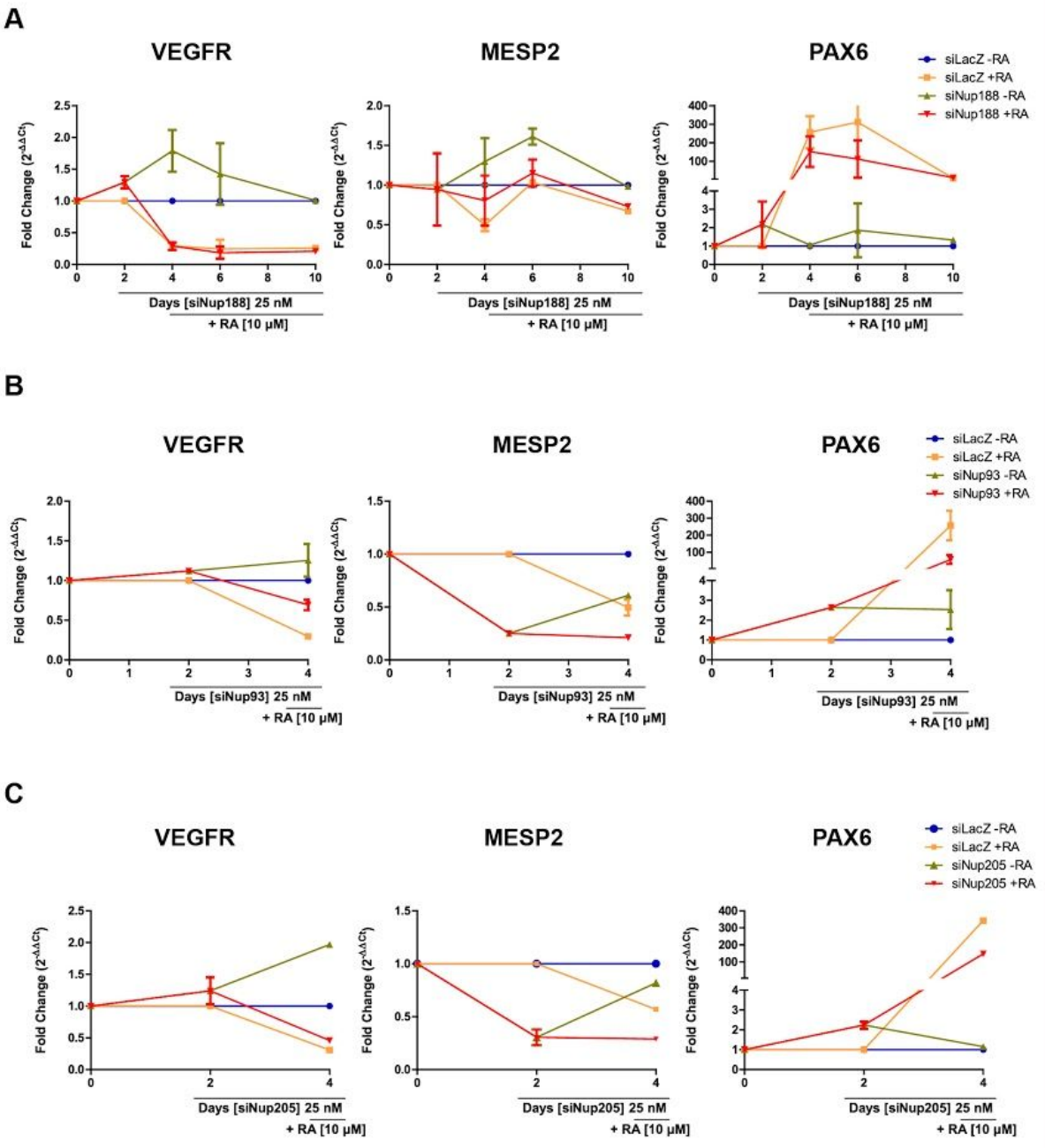

Fig. 4: Effect of the different knockdowns on VEGFR, MESP2, PAX6 gene expressions. Transcript levels of VEGFR, Mesp2 and Pax6 upon: (A) Nup188 knockdown. Data for day 0 to day 6 from N=2, n=6 replicates and day 8 from N=1, n=3 replicates. (B) Nup93 knockdown. Data for day 2 from N=1, n=3 and day 4 from N=2, n=6 replicates. (C) Nup205 knockdown. Data for day 2 from N=2, n=6 replicates, day 4 from N=1, n=3 replicates. Error bars represent SEM.

Nup205 depletion induces the formation of cellular aggregates

We independently performed Nup205 knockdown in NT2/D1 cells. Remarkably, this showed an aggregation of NT2/D1 cells in ~48 hrs, which eventually formed a cluster of cells that lifted off from the tissue culture plate. By ~72 hrs, most of the cells were part of such floating aggregates (Fig. 5A). The aggregates are of an average size of ~67 μm diameter (Fig. 5B). These aggregates reform ~24 hours after dissociating the cells using trypsin and reseeding (Fig. 5F). The aggregates reattach if the culture is incubated for an extended duration, while the cells spread out of the aggregate, potentially due to a dilution of Nup205 siRNA (Fig. 5H). Closer inspection of the physical morphology of aggregates revealed the presence of filopodia on its surface (Fig. 5G). Low adhesion conditions, like that offered by glass coverslips as compared to tissue culture-treated plastic (i.e., polystyrene that has been made hydrophilic), enhances the formation of aggregates (Fig. 5I). To test if aggregate formation is exclusive to systems capable of differentiation, we, therefore, depleted Nup205 in DLD1 cells - a terminally differentiated colorectal cancer cell line. Interestingly, Nup205 knockdown did not show comparable aggregates in DLD1 cells as that of NT2/D1(Fig. 6A). Furthermore, independent knockdowns of the Nup93 sub-complex i.e of Nup93, Nup188 or an independent Nup98 (not a part of Nup93 sub-complex) also did not show cellular aggregation. Taken together, the cellular aggregation property is therefore attributable to the exclusive loss of Nup205 in NT2/D1 cells.

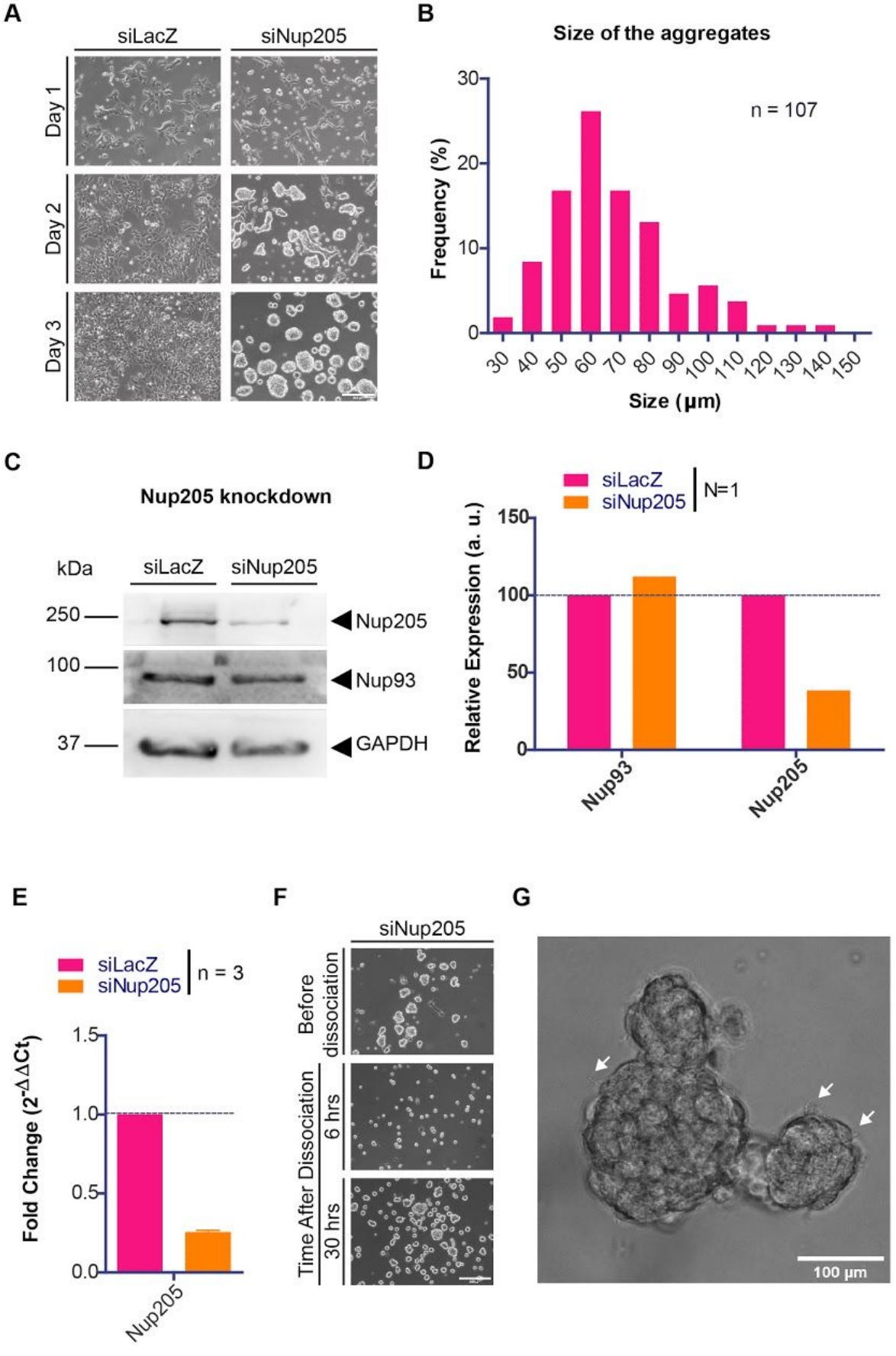
A
siLacZ
siNup205
Day 1
Day 2
Day 3
B
Size of the aggregates
n = 107
Frequency (%)
Size (µm)
C
Nup205 knockdown
kDa
siLacZ
siNup205
250
100
37
Nup205
Nup93
GAPDH
D
siLacZ
siNup205
N=1
Relative Expression (a. u.)
Nup93
Nup205
E
siLacZ
siNup205
n = 3
Fold Change (2-ΔΔCt)
Nup205
F
siNup205
Before dissociation
Time After Dissociation
6 hrs
30 hrs
G
100 µm

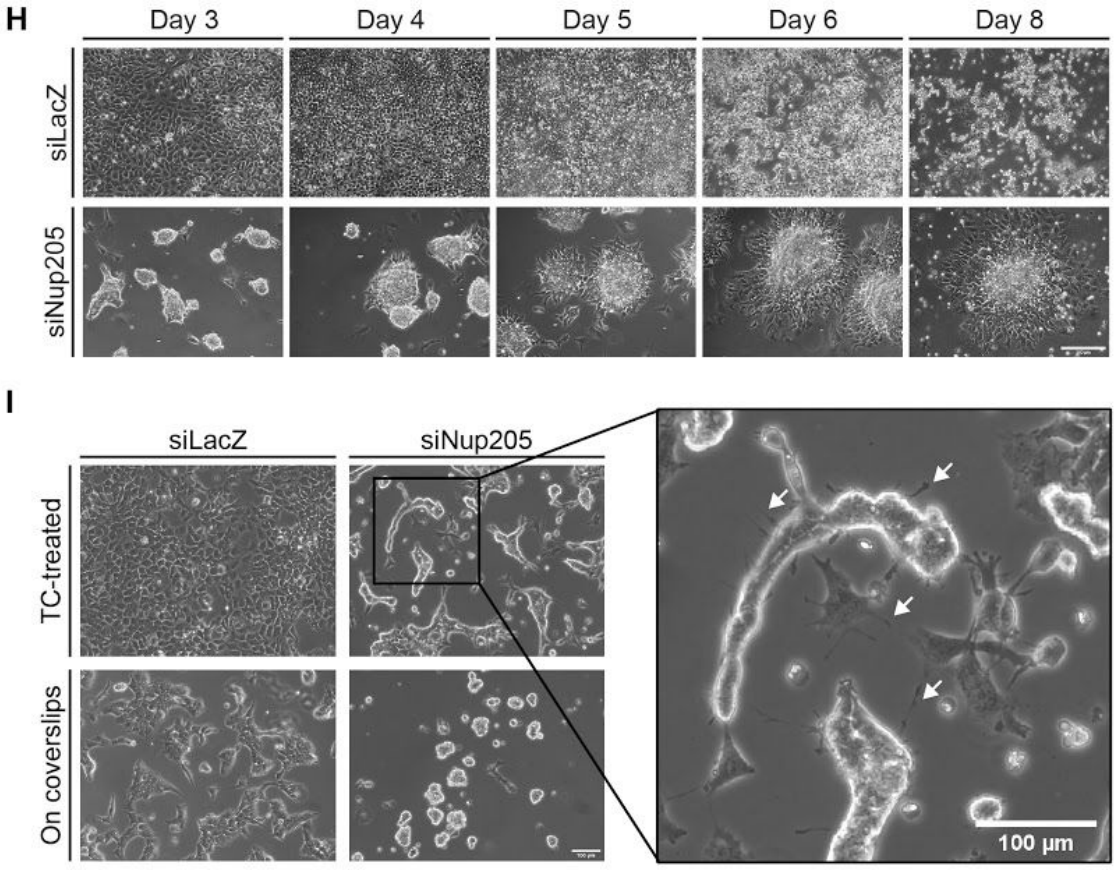

Fig. 5: Formation of aggregates upon Nup205 knockdown. (A) Phase contrast images of aggregate formation upon Nup205 knockdown in NT2/D1 cells. Scale bar = 200 µm. (B) Quantification of the diameter of the floating bodies. Data from n = 107 aggregates. (C) Protein level knockdown of Nup205 upon siRNA mediated knockdown and (D) its quantification. (E) Transcript level knockdown of Nup205 upon siRNA mediated knockdown. Data from n = 3 technical replicates. Error bars represent standard deviation. (F) Reformation of aggregates after trypsin mediated dissociation. Scale bar = 200 µm. (G) Morpohology of a floating body. Arrows indicated filopodia. Scale bar = 100 µm (H) Loss of aggregation phenotype after extended days in culture. Scale bar = 200 µm. (I) Enhanced formation of the aggregates on coverslips after 48 hrs of knockdown. Scale bar = 100 µm. (Zoomed image) Arrows indicate filopodia. Scale bar = 100 µm.

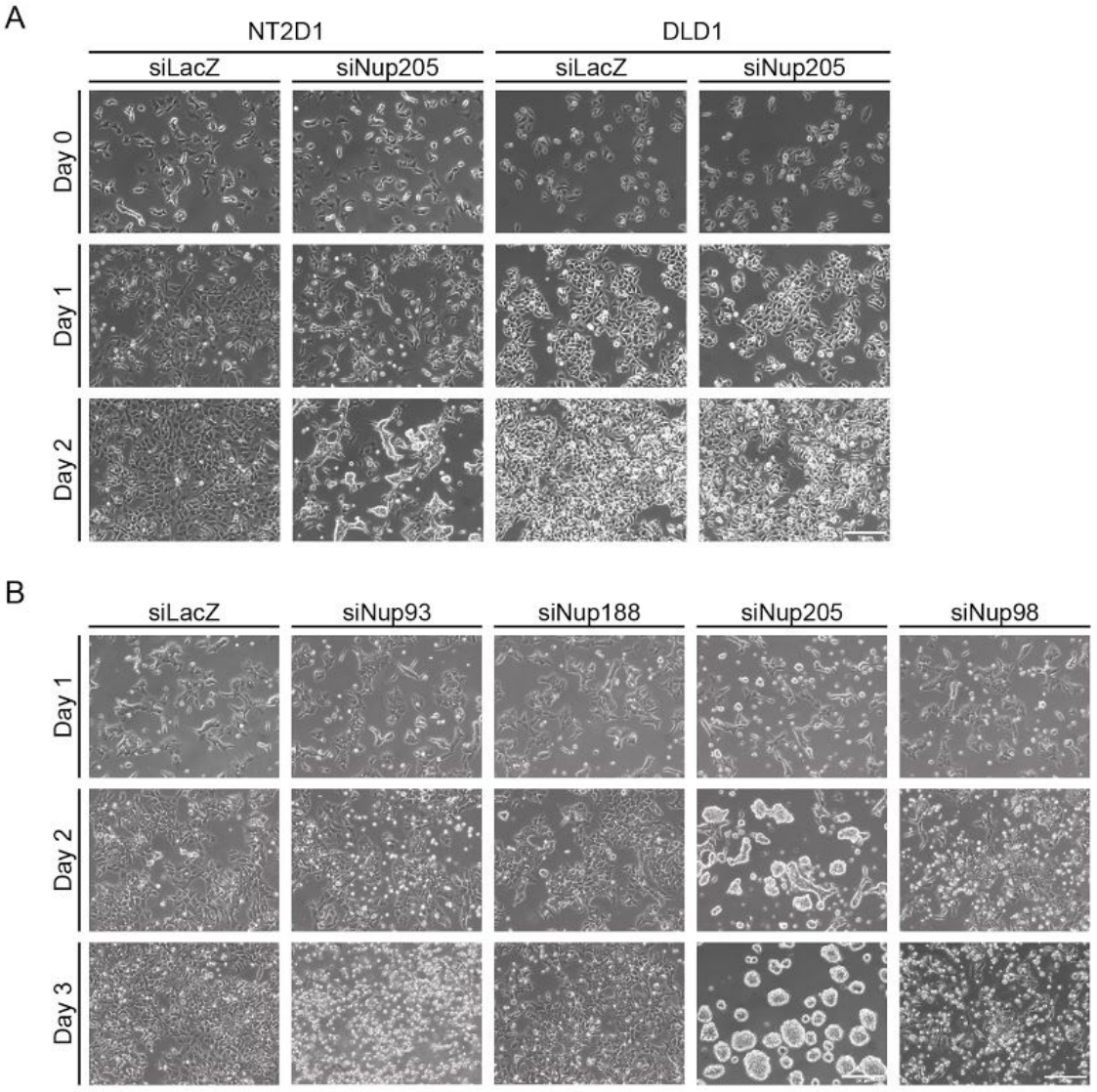

Fig. 6: Specificty of the aggregation phenotype. Phase contrast images of (A) Nup205 knockdown in the two cell lines, NT2/D1 and DLD1. Scale bar = 200 µm. (B) knockdown of the different nucleoporins in NT2/D1 cells. Scale bar = 200 µm.

Generation of shRNA constructs for the stable depletion of Nup205

To assess whether the phenotype seen upon siRNA mediated knockdown of Nup205 is an off-target effect of the siRNA, we generated stable shRNA clones of Nup205. We designed two sets of primers: one based on the existing Nup205 siRNA sequence and one based on a new siRNA sequence - referred to as sh1Nup205 and sh3Nup205 respectively. pLKO-Tet inducible vector was used as the vector backbone. The forward and reverse strands of both the shRNA oligos were annealed and ligated into the vector, and double digested with Age1 and EcoR1 restriction enzymes (Fig. 7A, 4B). Successful digestion by both restriction enzymes released a ~1.8 kb fragment from the vector, leaving sticky ends for the ligation of the annealed oligos. The ligated constructs were transformed into *E.coli* DH5α competent cells, cultured, and the plasmids were isolated. The plasmid contains multiple Xho1 digestion sites (Fig. 7C). Proper insertion of the shRNA sequence would result in two bands near 100 bp - 200 bp region, whereas the original vector would release just one fragment of ~190 bp in that region, when digested by Xho1. Xho1 digestion on the isolated plasmids revealed positive clones for both shRNAs (Fig. 7D). Positive clones of sh1Nup205 and sh3Nup205 were obtained as verified by sequencing results (see Appendix).

Transcription factors enriched at Nup205 promoter region

To understand the potential mechanism underlying the roles of Nup205 in inducing cellular aggregation, we examined different transcription factors enriched at the transcription start site (TSS) of the NUP205 gene. Analysis using ChIP-Atlas revealed MYCN, YY1 and CTCF as key transcription factors enriched at the promoter region of NUP205. We also tested the occupancy of these transcription factors on the other Nup93 subcomplex proteins from publically available ChIP-Seq datasets (Fig. 8A-C). Nup205 showed enrichment peaks of all the three transcription factors at its promoter. Nup93 showed enrichment for c-Myc, while Nup188 showed enrichment for both YY1 and c-Myc. From ChIP-Seq data on Nup205, CTCF was found to colocalize with 1) SMC3 and Rad21 (both components of cohesin) at the promoter region and gene body and 2) ZNF143 at the promoter region (Fig. 8D).

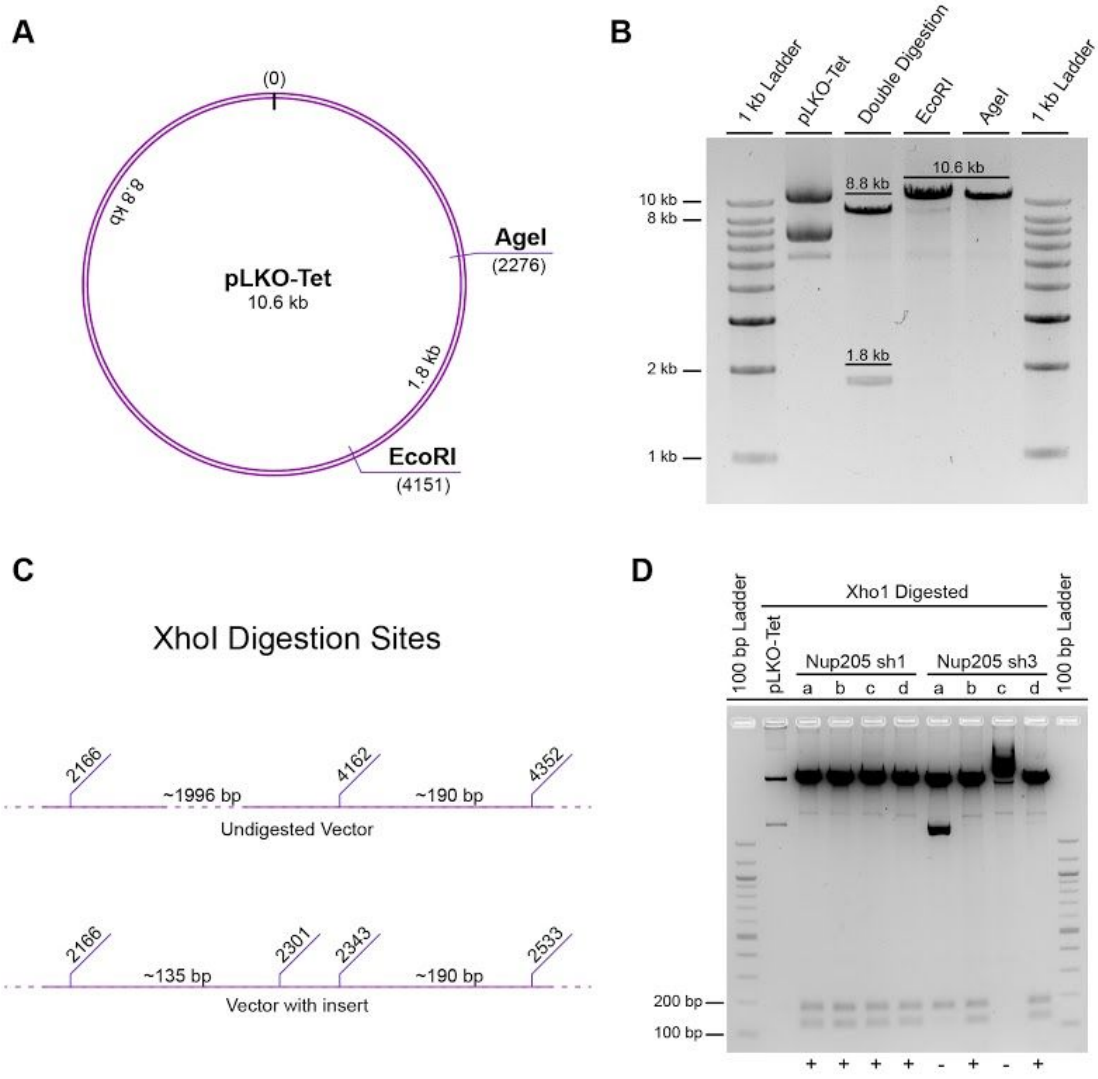

Fig. 7: Generation of Nup205 shRNA constructs. (A) Representative diagram showing the location (in brackets) of AgeI and EcoRI restriction digestion sites in the pLKO-Tet empty vector. (B) 0.8% Agarose gel depicting the release of the 1.8 kb fragment following digestion using AgeI and EcoRI. (C) Representative diagram depicting the different XhoI sites before and after insertion of the shRNA oligos. The size of the fragments that are released upon XhoI digestion are mentioned on the lines, which represent the plasmid. (D) Agarose gel image showing release of fragments upon XhoI digestion. Positive clones are labelled with a '+' beneath the lane.

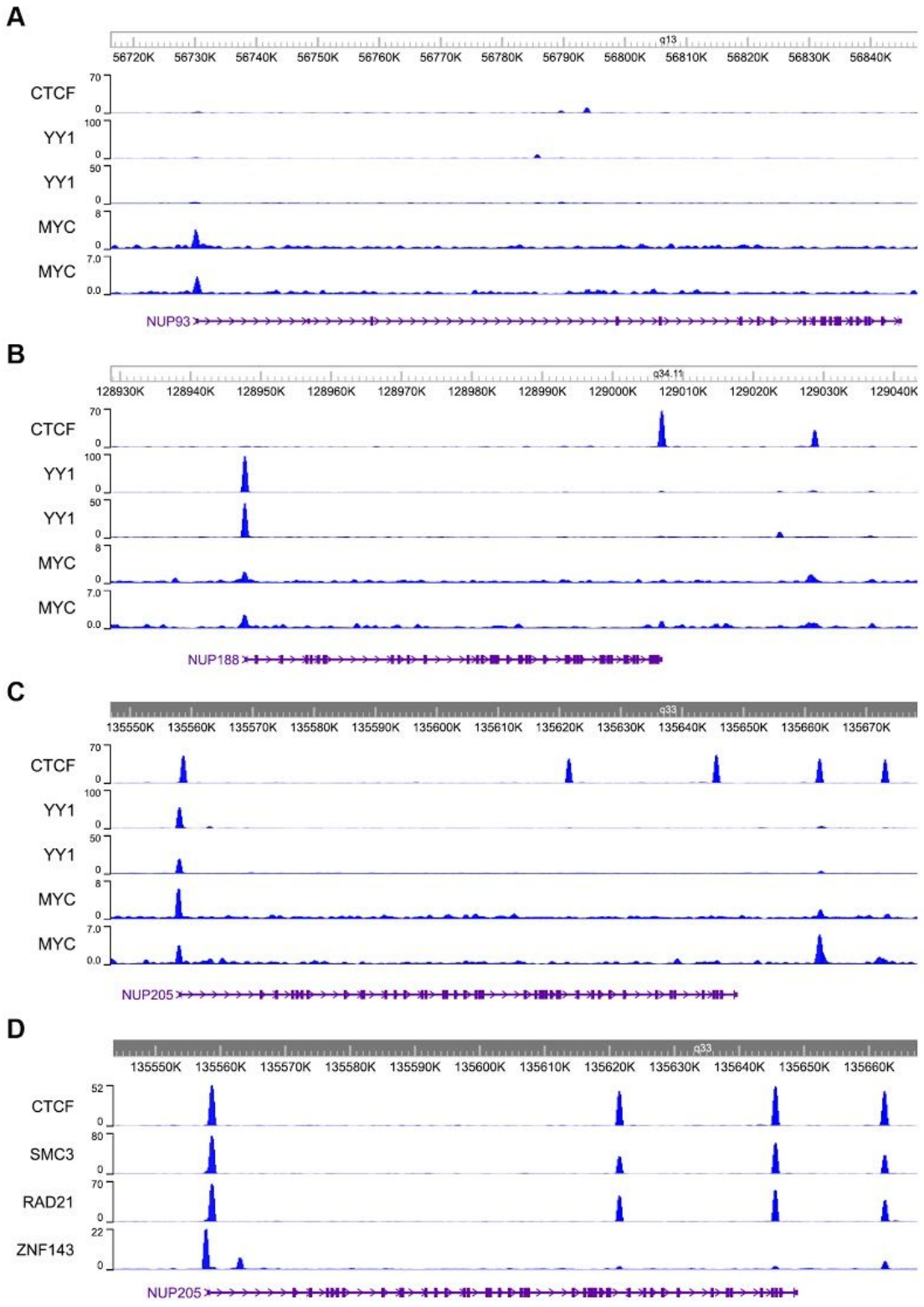

Fig. 8: Enrichment of different transcription factors at the nucleoporin genes. (A-C) ChIP-Seq data showing enrichment of transcription factors on NUP188, NUP93 and NUP205 respectively. (D) Enrichment peaks for CTCF, SMC3, Rad21 and ZNF143 for Nup205. Major ticks on the ruler represent a genomic distance of 10 kb. Lenght and position of the genes are representated by the purple lines below the plots.

In order to understand the biological relevance of the presence of these multiple transcription factors at Nup205 promoter region, we asked if these transcription factors show a co-occupancy in other systems as well. In silico analyses based on ChIP data revealed a cell type-specific pattern of co-occupancy in pluripotent cells, wherein YY1 and CTCF show a large overlap in their co-occupancy profiles, while in neural cell types - YY1 shows a co-occupancy with MYC but not CTCF. Furthermore, ZNF143 also shows a co-occupancy with YY1 and Notch1 in pluripotent cells. In summary, the promoter region of Nup205 shows enrichment of various transcription factors that are involved in both genome organisation and cell fate determination.

Decrease in lamin A/C levels upon RA treatment

The increase in lamin A/C levels serves as a useful marker of stem cell differentiation (Constantinescu et al., 2006). Interestingly, differentiated neuronal cells show reduced levels of lamin A/C (Takamori et al., 2018). Lamin B1 also modulates differentiation into neurons (Mahajani et al., 2017). To assess the status of the different lamin subtypes in the NT2/D1 differentiation system, lamin levels were assessed upon 8 days of RA treatment. As shown previously, in differentiating NT2/D1 cells, lamin A/C levels decrease (~40%) by Day 8, with a marginal increase in lamin B1 (~17%) and lamin B2 (~19%)(Fig. 9A, B). We tested if lamin knockdown affects the morphology of NT2/D1 cells. Phase-contrast images of lamin knockdowns show that at ~48 hrs, lamin B1 knockdown potentially induces cell aggregation (Fig. 9C).

Effect of matrix stiffness on differentiation

Extracellular matrix provides various cues that guide cellular differentiation. Mechanical stiffness dictates cell fates in naive mesenchymal stem cells (Engler et al., 2006). Therefore, we examined if altered matrix stiffness affects RA induced cellular differentiation. Towards this end, we selected a substrate stiffness of ~2 kPa collagen-coated PDMS matrices as the softer substrate, while collagen-coated glass coverslips served as the stiffer substrate. NT2/D1 cells were cultured on the substrates, supplemented with [RA] 10 μM, every ~48 hours. They were imaged, followed by the quantification of cell surface area. On both the substrates, RA

treatment showed a significant increase in the mean cell surface area, accompanied by an increase in heterogeneity in the area of the cells (Fig. 10A, 10B). However, the effect of RA on increasing cell area was much more pronounced on stiffer substrates than softer substrates (Fig. 10D). In the absence of RA, there was no significant effect of stiffness, and both substrates had similar cell areas (Fig. 10C).

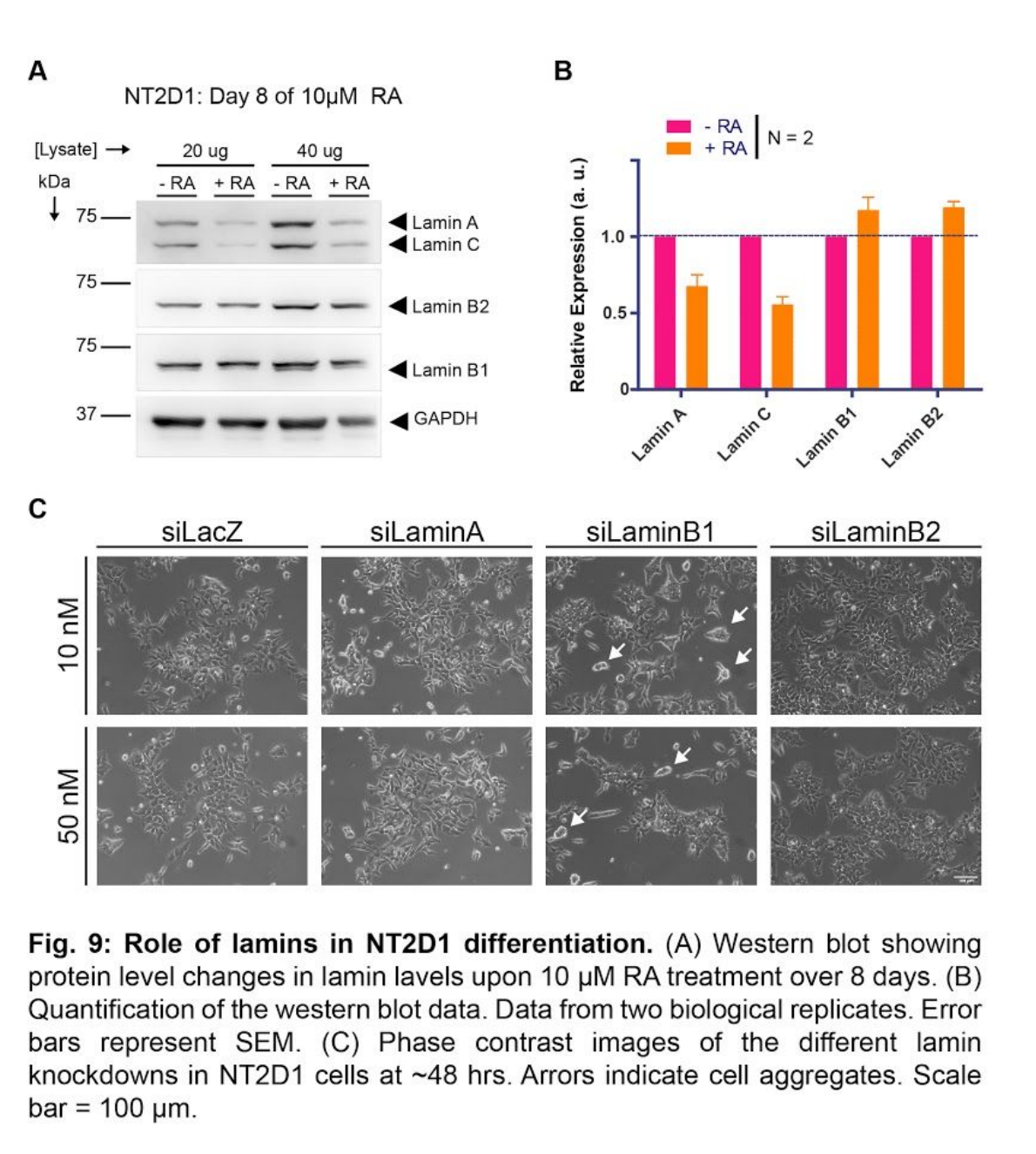

Fig. 9: Role of lamins in NT2D1 differentiation. (A) Western blot showing protein level changes in lamin lavels upon 10 μM RA treatment over 8 days. (B) Quantification of the western blot data. Data from two biological replicates. Error bars represent SEM. (C) Phase contrast images of the different lamin knockdowns in NT2D1 cells at ~48 hrs. Arrors indicate cell aggregates. Scale bar = 100 μm.

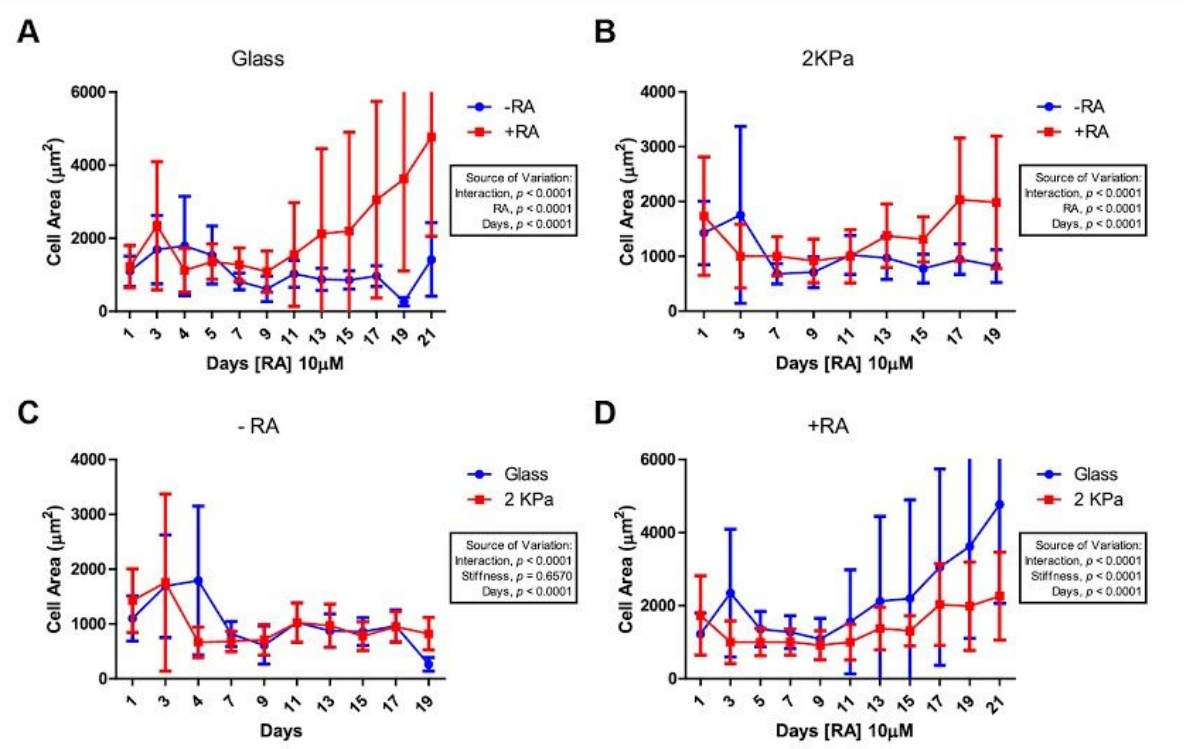

Fig. 10: Changes in NT2D1 cell area with respect to matrix stiffness and RA: (A), (B) shows the effect of RA on NT2D1 cells within the stiffness regimes of glass and 2 KPa. (C), (D) shows the effect of matrix stiffness in either control cells or in RA treated cells. Each data point is taken from n=~30 cells, N=1. Error bars represent standard deviation. Statistical significance measured using mixed model two-way ANOVA. *p*-Values given in inset boxes.

In summary, we show that the Nup93 subcomplex genes (Nup93, Nup188 and Nup205) regulate key genes involved in maintaining pluripotency, and can modulate their gene expressions during RA-mediated differentiation in NT2/D1. These nucleoporins also play a role in regulating expression of lineage-specific genes, and Nup205 plays a unique role in cell aggregation. We also show that RA-induced differentiation differentially affects lamins, and how mechanical stiffness can affect parameters representative of neuronal differentiation.

DISCUSSION

NT2/D1 is a human pluripotent embryonal carcinoma cell line. BMP-7 (Bone Morphogenic Protein-7) induces an epithelial phenotype in these cells, whereas treatment with RA (retinoic acid) induces neuronal differentiation. Terminally differentiated neurons derived from these cells have been validated to be functional neurons (Nelson et al., 2002). RA functions through two receptor families from the nuclear receptor superfamily: retinoic acid receptors (RARs) and retinoid X receptor (RXRs). These form RAR/RXR heterodimers and RXR/RXR homodimers, which bind to retinoic acid response elements (RAREs) present on the target genes. Binding of the ligand RA leads to the dissociation of corepressor proteins and the recruitment of coactivators, resulting in transcriptional activation. We characterised RA induced changes in NT2/D1 by assessing the levels of the pluripotency markers, Oct4, Sox2 and Nanog. Lowered levels (~95%) of Oct4 and Nanog were indicative of differentiation (Fig. 1D). Sox2 levels fluctuate across days and were slightly lowered (by ~35%) by the end of day 8 (Fig. 1D). The persistence of Sox2 can be attributed to the role of Sox2 in maintaining neural stem cells and neural progenitor cells (Bowles et al., 2019; Ellis et al., 2004; Ferri et al., 2004). This is suggestive of commitment to neuronal cell fate. Increased levels of Pax6 confirms this (Fig. 1G) (Heins et al., 2002). Accordingly, VEGFR (Vascular Endothelial Growth Factor Receptor), a marker for endothelial cells, shows a decrease in levels. The levels of mesodermal marker Mesp2 (Mesoderm posterior protein2), fluctuate and remain slightly lower (~30%) by the end of day 8 of RA treatment. Although NT2/D1 cells differentiate into a neuronal lineage, these cells express genes that determine a mesodermal lineage even in the absence of mesodermal differentiation (Gokhale et al., 2000). Tbx6 is a transcription factor that modulates Mesp2 levels through Notch signaling in presomitic mesoderm during somitogenesis (Yasuhiko et al., 2006). It is of interest to note that Tbx6 is also involved in regulating Sox2, acting as a switch between mesodermal and neural cell fate for axial stem cells (Takemoto et al., 2011). Notch signaling is implicated in inhibiting neuronal differentiation (Nagao et al., 2007). Loss-of-function mutation in Notch led to a cell fate switch whereby cells destined to become epidermal cells switched to a neuronal cell type

(Artavanis-Tsakonas et al., 1999). Abrogation of Notch-Delta signaling shows an increase in the number of neurons produced from a neurosphere, at the expense of other cell fates (Grandbarbe et al., 2003). On the other hand, Mesp2 suppresses Notch signaling (Sasaki et al., 2011). Taken together, the persistence of Mesp2 is potentially involved in the suppression of Notch, in order to promote a neuronal differentiation program. Once differentiation into neuronal lineage upon RA treatment was established, we investigated the effect of depleting individual genes of the Nup93 sub-complex namely - Nup93, Nup188 and Nup205 on differentiation. Nucleoporins constitute the nuclear pore complex (NPC) and are generally involved in nucleocytoplasmic transport (Bestembayeva et al., 2015). In addition to nuclear transport (import and export), nucleoporins are also involved in gene regulation and DNA damage repair. Nup93 represses HOXA gene expression assisted by its direct interactors Nup188 and Nup205 in the differentiated cell line DLD1 (Labade et al., 2016). In NT2/D1 cells, Nup93 has been implicated in regulating HOXA gene expression throughout the differentiation paradigm (Labade et al., 2019). Hence it was imperative to understand the regulatory role of Nup93, and its interacting partners Nup188 and Nup205 on RA mediated neuronal differentiation.

To a large extent, knockdowns of the three nucleoporins did not affect the expression levels of the one another, except for a decrease in Nup188 levels (~25%) upon Nup93 knockdown (Fig. 2). This is indicative of an absence of transcriptional level feedback between the three genes, whereby a decrease in one shows an increase in the others, that may potentially maintain the overall stoichiometry of the Nup93 sub-complex. The presence or absence of RA does not alter the expression levels of the three genes, suggesting that the Nup93 sub-complex is relatively stable throughout the course of differentiation (Labade et al., 2019). Therefore, the Nup93 sub-complex proteins potentially function as master regulators of differentiation. In the absence of RA, depletion of Nup93 sub-complex genes increases Oct4 and Nanog levels by day 4, and Sox2 by day 2 followed by a return to basal levels by day 4 (Fig. 3). The overall increase in transcriptional levels of the pluripotency markers Oct4, Sox2, and Nanog upon knockdown suggests that Nup93 sub-complex genes transcriptionally repress their levels, and their knockdown stimulates cells towards a

more pluripotent state. The fact that addition of RA completely counteracts the effect of Nup188 knockdown on Oct4, Sox2 and Nanog levels, but not the effect of Nup93 knockdown, suggests that 1. Nup188 and Nup93 could have non-redundant/mechanistically distinct roles in repressing the genes and 2. the effect of RA, is in between the effect of Nup93 and Nup188. Similar to the levels of pluripotency markers, the levels of VEGFR, Mesp2 and Pax6 increase upon Nup188 knockdown, and the addition of RA decrease their levels, except for Pax6, which shows an increase, consistent with its elevated levels characteristic of a switch to neuronal cell fate. The increase in VEGFR and Mesp2 suggests that the cells are poised for differentiation into any of the three different germ layers, even if an increase in a single marker is insufficient to arrive at such a conclusion. Expression analysis of other lineage markers upon knockdown may be useful to support the statement. However, as shown by Simões and Ramos, persistence of mesodermal gene expressions in NT2/D1 cells were not accompanied by mesodermal differentiation, indicating that the expression of genes of a certain lineage does not guarantee cellular differentiation into the particular lineage (Simões and Ramos, 2007). Nup93 and Nup205 knockdowns, on the other hand, show a decrease in Mesp2 levels at day 2 (~70%) and day 4 (~30%)(Fig. 4). This further underscores a difference in the regulation pattern between Nup93 and Nup188. The overall trend in expression levels across both pluripotency markers and lineage markers reveal that Nup93 knockdown and Nup205 knockdown have similar effects, suggesting that they both might be either functioning together and/or have redundant roles in gene regulation.

However, the knockdown of Nup205 induces NT2/D1 cells to aggregate. Upon Nup205 knockdown, the cells come together forming aggregates that lift off by ~72 hrs lift off from the culture plate into floating aggregate bodies (Fig. 3A). Reformation of the aggregates after dissociation shows that these floating bodies contain live cells. Furthermore, the cells retain the capacity to form the aggregates and actively try to maintain that state (Fig. 5F). Cells in culture for an extended duration reattach to the culture plate and start spreading out of the aggregate like normal cells. This suggests the necessity of a constant pulse of Nup205 siRNA to maintain these

aggregates (Fig. 5H). The presence of filopodia on both the adherent cells and the aggregates and its overall morphology resembled that of neurospheres (Fig. 5G, 5I). Neurospheres are three-dimensional cell aggregates that form from neural progenitor/stem cells when grown on non-adhesive surfaces in the absence of serum (Ladiwala et al., 2012). As shown by Ladiwala et al., filopodia on adherent cells assist cell movement and adhesion to neighbouring cells. Their study concluded that in single-cell suspension of neural stem cells, a minimum interaction time of ~5 s between filopodia from two different cells would lead to irreversible cell-cell adhesion. This could explain the reformation of the aggregates after dissociation by trypsinization (Fig. 3F). Since culturing cells on a low adhesion surface is a well-established method of generating neurospheres (Yang et al., 2015), we studied the effect of culturing cells on glass coverslips, which are of lower adhesive property compared to plastic (hydrophilic polystyrene ones). Growing the cells on glass coverslips visibly enhanced the aggregation phenotype. This further suggests that Nup205 knockdown potentially induces a generic pathway involved in neurosphere formation, as factors affecting known neurosphere formation also amplifies the knockdown phenotype. If this is the case, and neurosphere formation is limited to cells that have the capacity to become neural progenitor/stem cells, then knocking down Nup205 in other differentiated systems should not show aggregation. Nup205 knockdown in DLD1, a terminally differentiated human colorectal adenocarcinoma, does not show neurosphere formation or cell aggregation (Fig. 6A). In order to conclusively implicate Nup205 in neurosphere formation, similar phenotypes have to be tested in other pluripotent systems like iPSCs and neural stem cells upon Nup205 knockdown. Another approach would be to perform stable inducible knockdowns of Nup205 using an shRNA. Furthermore, a rescue experiment will also be useful to determine the specificity of Nup205 in the cell aggregation phenotype. Of note, the knockdown of the other nucleoporins of the Nup93 subcomplex, Nup93 and Nup188, did not lead to the phenotype. This suggests that Nup205 plays a role that is exclusive to itself. Until evidence points toward an off-pore localisation of Nup205, it is likely that Nup205 is involved in repressing genes that could trigger the neurosphere formation pathway by tethering them to the nuclear periphery. This is just a speculation as of now.

Upon analysing the different transcription factors at the TSS of Nup188, Nup93 and Nup205, we detected the enrichment of YY1, c-Myc, CTCF, SMC3 and ZNF143 on Nup205 promoter. YY1 and CTCF are involved in maintaining looping interactions that are necessary during early commitment to a neural progenitor cell fate (Beagan et al., 2017). ZNF143, along with CTCF and Cohesin (whose two subunits SMC3 and Rad21 are found to be enriched in Nup205), modulates chromatin loop interactions and associates with lineage-specific gene expression (Bailey et al., 2015). Both CTCF and Cohesin regulate gene expression by mediating long-distance interactions, especially in cell fate commitment, such as the formation of neural progenitor cells from embryonic stem cells (Phillips-Cremins et al., 2013). Myc is involved in promoting neuronal differentiation by inhibiting Notch signaling, which as previously discussed allows for increased neurogenic cell division (Zinin et al., 2014). Coincidently, ZNF143 colocalizes with NOTCH1 in pluripotent stem cells. Taken together Nup205 is transcriptionally regulated in the context of neural progenitor cell formation and differentiation.

Lamin levels were found to be altered upon prolonged RA treatment. After 8 days of RA, lamin A and lamin C showed decreased protein levels by day 8. Generally, lamin A levels are lower in undifferentiated cells and higher in differentiated cells. However, here we see an opposite trend wherein the level of lamin A decreases upon RA-mediated differentiation. Also, lamin A/C promoter has a RARE domain, where RAR/RXR dimer binds upon activation by the ligand RA and increases gene activity. Nevertheless, we detected a decrease in lamin A/C levels. This could be explained based on the context of our system, as NT2/D1 upon RA treatment differentiates towards a neuronal phenotype. Neurons have low levels of lamins, and hence lower lamin A /C levels could be indicative of the cell fate that NT2/D1 is differentiating into. A neuronal differentiation program could have multiple factors affecting the regulation of lamin A/C, possibly counteracting the direct effect of RA on its promoter. Phase-contrast images of the different lamin knockdowns revealed that by ~48 hrs lamin B1 knockdown showed a phenotype where the cells form diffused but apparent cell aggregates. Some of these clusters of cells resemble attenuated

versions of clusters after ~24 hrs of Nup205 knockdown, and these do not form floating aggregates and cells grow normally with time. This suggests a link between Nup205 and lamin B1 in regulating a single/set of pathway(s) involved in the aggregate formation, with lamin B1 involved in regulating a partial set of genes that Nup205 regulate, as we do not see the complete aggregation phenotype upon lamin B1 knockdown. Further analysis of how lamin knockdowns affect the expression of both pluripotency markers and lineage markers in the context of RA mediated differentiation will help us elucidate the role of lamins in differentiation.

Another factor that can affect differentiation is matrix stiffness. Stiffer matrices (~40 kPa) promote osteogenesis in stem cells, compared to softer matrices (~1 kPa) that promote neurogenesis (Engler et al., 2006). The biological context of tissue stiffness plays a major role in regulating differentiation potential. Also, lamin A levels to scale with tissue stiffness (Swift et al., 2013) (lower stiffness correlates with lower lamin A levels), and since RA mediated differentiation lowers lamin A levels in NT2/D1 cells, it suggests that softer matrices might be a better context for neuronal differentiation in our system. As a preliminary analysis, we examined cell spreading upon RA treatment when grown on different stiffnesses, as neuronal differentiation leads to a change in cellular morphology. In general, RA treatment shows an increase in cell area on both glass and soft (~2 kPa) matrix (Fig. 10 A, B). In the absence of RA, the cell areas were similar between both glass and matrix, and there was no significant correlation between stiffness and area (Fig. 10C). Whereas in RA treated cells, glass showed much more cell spreading than on softer matrices (Fig. 10D). The reason why we do not see even a basal change in cell areas between glass and 2 kPa in the absence of RA could be that the cells multiply and reach confluency, restricting the area available for the cells to spread. In the case of RA treated cells, due to differentiation, their capacity to multiply is reduced and the total cell number is lower giving the cells enough space to spread out and reach their natural cell spread area. And therefore, in the absence of RA, the cell areas observed could be an artefact of confluency, whereas lower confluency in RA treated cells reveal the proper cell spread.

In iPSCs, neuronal differentiation leads to an increase in the cell area from day 3 to day 12 of differentiation (Kang et al., 2017), and matrix with lower stiffness leads to neuronal differentiation (Engler et al., 2006). Taken together, these suggest an increase in cell area on lower stiffness compared to higher stiffness, upon RA treatment. However, we see the opposite trend (Fig. 10D). This could be attributed to the effect of matrix on cell spreading, where stiffer matrices lead to better spreading (Yeung et al., 2005). Therefore, the direct effect of the matrix could be greater than the effect of differentiation on the cell area and hence glass shows greater cell spreading than 2 kPa matrix. Analysis of lineage and pluripotency markers will help elucidate the role of matrix stiffness on RA mediated differentiation in these cells.

In conclusion, we show that the Nup93 sub-complex proteins Nup93, Nup188 and Nup205, which are present in the inner scaffold of the nuclear membrane, regulate expression of genes involved in the maintenance of pluripotency and lineage. To determine if this regulation is based on repositioning of the gene loci to the nuclear periphery, similar to how Nup93 tethers and represses HOXA gene cluster at the nuclear periphery (Labade et al., 2019), FISH should be performed. Analysis of gene expression profiles upon the knockdown of Nup93, Nup188 and Nup205 using RNA-Seq will reveal whether these nucleoporins are major regulators of cell fate determination. Formation of cell aggregates upon Nup205 depletion puts Nup205 as a potential upstream inhibitor of pathways involved in neurosphere formation. Inhibition of proteins involved in those pathways should thus abrogate the phenotype seen upon Nup205 depletion. This will have to be investigated. Considering that lamin levels are altered upon RA-induced differentiation, the impact of lamins on neuronal differentiation should be probed by looking at gene expressions of pluripotency and lineage markers upon their depletion. With regards to how low adhesion surfaces promote Nup205 depletion-induced phenotype, and previous evidence suggesting the role of mechanosignalling in both modulating lamin levels and differentiation, the role of mechanosignalling in modulating RA-mediated differentiation should also be investigated. These will provide insight towards how the nucleoporins could function along with inputs from both lamins and extracellular signals in regulating gene expressions.

MATERIALS AND METHODS

Cell Culture

Frozen cells were thawed at 37°C using a water bath and the contents were transferred into a 60 mm dish containing 4 ml of media, prewarmed at 37°C, and incubated for 6 to 7 hours, at 37°C, with 5% CO_2. The media was changed to remove the cryoprotectant DMSO. The flask was incubated overnight at 37°C, with 5% CO_2 concentration. Cells were incubated till confluent.

Cell Splitting

NT2/D1 cells were cultured in Dulbecco's Modified Eagle's Medium supplemented with 10% FBS (Sigma F2442), 100U/ml Penicillin/ 100µg/ml Streptomycin and 2mM Glutamine at 37°C and 5% CO_2. Cells were trypsinized (0.05% trypsin) and subcultured when confluent. Retinoic acid (Sigma R2625) was dissolved in DMSO and was directly added to the medium. RA is light sensitive and was handled in conditions of reduced light. For all experiments, 10µM Retinoic acid was used and was replenished every 2 days. Untreated cells were collected at day 0 of RA addition. For prolonged knockdown experiments, cells were reseeded as mentioned to maintain the efficiency of the knockdown.

siRNA mediated transient knockdown

0.2 x 10^6 cells were seeded in a 35mm dish and 24 hr after seeding, siRNA transfection was performed. 5µl RNAiMax transfection reagent was added to 250µl OptiMEM, and the required volume of siRNA was added to 250µl OptiMEM in a separate tube. A short vortex and spin were given and the vials were incubated at RT for 5 min, after which the contents of the vial with RNAiMax were added to the other vial. A short vortex and spin were given. After 30 min incubation, this mixture was added to 1.5ml medium to achieve final concentration. As control, siLacZ (Dharmacon) was used. The medium was changed 24 hr post addition.

siRNA Oligo sequence-

Nup93 - 5’AGAGTGAAGTGGCGGACAA3′

Nup188 - 5′GCCTTTCTGCGCTTGATCACCACCC3′

Nup205 - 5′AGAUGGUGAAGGAGGAAUAUU3′

LaminA/C - 5’CAGUCUGCUGAGAGGAACA3’

LaminB1 - 5’AGACAAAGAGAGAGAGAUG3’

LaminB2 - 5’GAGCAGGAGAUGACGGAGA3’

RNA Isolation and cDNA synthesis

Adherent cells were washed with 1X PBS. 500µl TRIzol was added to each well of a 6-well plate and pipetted 5-6 times. The contents were then transferred to a 1.5 ml vial and vortexed for 15 seconds. Then the vial was incubated at room temperature for 5 minutes. After incubation, 100µl chloroform per 500µl Trizol was added and mixed by vigorous vortexing. After 15 min incubation, samples were spun down at 4°C for 15 min at 12,000g. The aqueous layer was separated and an equal volume of Isopropanol was added. Samples were mixed by inverting the tube around ~25 times and incubated for 15 min at RT and spun down at 4°C/12000g/15 min. Pellet was washed twice with 70% ethanol at 4°C/12000g/15 min. Ethanol is carefully removed and the RNA pellet was air-dried and resuspended in nuclease-free water (NFW, Sigma). The quality of RNA was assessed on NanoDrop™ with 1µl RNA. 1µg of RNA was used to prepare cDNA using Thermo Scientific™ Verso cDNA Synthesis Kit in a 20µl reaction.

RNA Mix

Reagent	Volume (µl)
RNA (1 µg)	1
Oligo dT	1
NFW	3
Total	4

Verso Reverse Transcription Mix (RT mix)

Reagent	Volume (µl)
5x cDNA Synthesis buffer	4
dNTP mix	2
Verso RT enhancer	1
Verso Enzyme mix	1
Nuclease free water	7
Total	15

The RNA mix was heated at 70°C for 5 min and quickly chilled in ice for 5 min. 15µl of RT mix was added to the RNA mix. PCR scheme used for cDNA Synthesis is as follows:

Step	Temperature (°C)	Time (min)
Annealing	25	15
Extension	42	60
RT Enzyme Inactivation	70	5
Hold	4	-

Prepared cDNA was diluted 1:1 with NFW. RT-qPCR was set up with KAPA SYBR Green in a 5µl reaction.

Primer Master mix for 1 reaction (well) in the RT-PCR 96-well plate:

Reagent	Stock Concentration	Final Concentration	Final Volume
Kapa SYBR Green	2 X	1 X	2.5 µl
Primer (F+R)	10 µM	0.4 µM	0.2 µl
NFW	-	-	1.3 µl
Total	-	-	5.0 µl

The components were added in the following order: NFW, Primer, SYBR Green. Give a short vortex and spin after the addition of SYBR Green. 4 µl of the Primer Master mix was first added to each well, followed by the addition of 1 µl of diluted cDNA. The plate was sealed with a micro-sealer with the help of soft tissue by gently pressing over the sides and wells of the plate. The sealed plate was spun at 800 RPM for 2 minutes at RT. PCR was performed on BIORAD real-time PCR. Ct values for each sample were double normalized to internal control and reference, respectively.

The qRT-PCR instrument was run according to the following program:

- 95 °C - 3 minutes (Hot start reaction)
- 95 °C - 20 seconds (Denaturation)
- 60 °C - 1 minute (Annealing and Data acquisition)
- Repeat cycle 35x (b., c.)
- 65 °C to 95 °C, 0.5 °C/cycle: Determination of melt curve
- 4 °C - Hold for infinity

Immunofluorescence Assay

Cells were washed twice with 1X PBS for 5 minutes each (all further PBS washes are 5 mins each). 1 ml 4% PFA was added to each well and incubated for 10 minutes at RT. The cells were washed twice with 1 ml 1X PBS. Cells were permeabilized with 1 ml 0.5% TritonX-100 for 10 minutes. Cells were washed twice with 1 ml 1X PBS. Cells were blocked with 1% BSA in 1X PBST (1X PBS +0.1% Tween 20) for 1 hr at RT. Cells were washed twice with 1 ml 1X PBS, followed by incubation of the coverslips in 50 µl of primary antibody diluted in 0.1% BSA (in PBST) for 90 mins at RT in an air-tight humidified chamber, by inverting the coverslip onto an antibody dropped on a piece of parafilm. Coverslips were washed thrice in 1X PBS to remove excess primary antibody and then were incubated with 50 µl of secondary antibody diluted in 0.1% BSA (in PBST) for 1 hr at RT in a similar manner. All the steps from secondary antibody incubation are done in dark conditions. After the incubation, cells were washed thrice with 1ml 1X PBS and the cells were incubated with 1 ml DAPI (0.05 µg/ml) for 2 minutes at RT. The cells were washed

thrice with 1 ml 1X PBS. The coverslips were mounted on glass slides using 10 µl anti-fade and sealed.

Western Blotting

The cells were washed with 1X PBS once following which 50 ul of modified Radio Immunoprecipitation Assay buffer (RIPA with 1X Protease Inhibitor Cocktail) was added per 35 mm dish. Using a cell scraper, cells were thoroughly scraped off. This lysate was placed on ice for 5 mins. Then it was centrifuged at 4°C, 13,000 rpm for 15 minutes. The supernatant was collected into fresh vials and stored at -80°C or used immediately for protein estimation using Bicinchoninic Acid. For BCA, Pierce™ BCA Protein Assay Kit (#23225) reagents A and B and were diluted in a concentration of 50:1 (A:B). For the preparation of protein standards, 10ul standards and 200ul BCA mix were added. 5ul Modified RIPA buffer, 5ul 1X PBS and 200ul BCA mix were added as blank. For test samples, 5ul lysate was added to 5ul 1x PBS and 200ul BCA mix. All samples were made in duplicates. The plate was incubated at 37°C for 30 minutes and readings were taken on a spectrophotometer at 562 nm. Samples were prepared in a 1x Laemmli buffer with 20 µg protein (unless specified otherwise) and were heated at 95°C for 10 minutes after which it was loaded. Protein samples resolved by SDS-PAGE were transferred to polyvinylidene fluoride (PVDF) membrane then blocked using 5% skimmed milk in 1X TBST (Tris buffer saline, 0.1% Tween 20) for 1hr at RT. Primary antibodies were diluted in 0.5% milk in 1X TBST and were incubated overnight. The HRP-tagged secondary antibodies were diluted in 0.5% milk in 1X TBST. Blots were developed using enhanced chemiluminescence detection reagents (Amersham™ ECL™ Prime Western Blotting Detection Reagent kit (RPN2232). Images were acquired every 10s of exposure.

Generation of shRNA clones

pLKO-Tet (Tet-pLKO-puro, Addgene Plasmid #21915) was used as the vector backbone. Primers based on the following siRNA sequences were designed according to the user manual for the vector on Addgene.

Nup205 Oligo Name		**Sequence (5’ - 3’)**
siRNA 1		AGAUGGUGAAGGAGGAAUAUU
siRNA 2		GCCAGUGCUUAGGACUACUAA
shRNA 1 (sh1)	Forward	CCGGAGATGGTGAAGGAGGAATATTCTCGAGAATAT TCCTCCTTCACCATCTTTTTT
	Reverse	AATTAAAAAAGATGGTGAAGGAGGAATATTCTCGAGA ATATTCCTCCTTCACCATCT
shRNA 3 (sh3)	Forward	CCGGGCCAGTGCTTAGGACTACTAACTCGAGTTAGT AGTCCTAAGCACTGGCTTTTT
	Reverse	AATTAAAAAGCCAGTGCTTAGGACTACTAACTCGAGT TAGTAGTCCTAAGCACTGGC

The annealing reaction was prepared in 0.6 ml tubes:

	Nup205 sh1	**Nup205 sh3**
Forward Primer (100 µM)	4.5 µl	4.5 µl
Reverse Primer (100 µM)	4.5 µl	4.5 µl
NEBuffer 3	1.0 µl	1.0 µl
Total	10.0 µl	10.0 µl

The 0.6 ml tube containing the mixture is kept over boiling water with the help of a floater and the temp is allowed to reach RT naturally. Once it cools down, the annealed oligos are kept on ice and stored at -20 °C.

Restriction digestion of the empty vector pLKO-Tet was performed using the restriction enzymes AgeI Hf and EcoRI Hf simultaneously. Single digestion was also performed parallelly to validate the effectiveness of the individual enzymes. The entire reaction mix is prepared in a 1 ml tube and is incubated at 37 °C for 3 hours.

The enzymes are then inactivated at 65 °C for 20 mins. Once validated, the single digests may be further used to make the double digested product by sequentially digesting it with the other enzyme.

	Simultaneous DIgestion	**AgeI**	**EcoRI**
Vector (5.3 µg/µl)	2 µl	2 µl	2 µl
EcoRI HF	1 µl	-	1 µl
AgeI HF	1 µl	1 µl	-
10x CutSmart	5 µl	5 µl	5 µl
NFW	41 µl	41 µl	41 µl
Total	50 µl	50 µl	50 µl

For extracting the cut vector, the entire reaction volume is run on a 0.8% Agarose gel prepared in 1x TAE buffer with SYBR Safe (5 µl in 70 ml 1x TAE). Make sure that the gel is thick enough for the wells to hold the entire reaction volume. Run the gel at 120V. After running the gel, the 8.8 kb fragment is visualised over UV and the region containing the 8.8 kb fragment is cut out neatly using a clean scalpel and transferred into a 1.5 ml tube, whose weight has been measured beforehand, in order to know the weight of the cut gel piece. Following this, the plasmid was extracted from the gel using QIAGEN QIAquick Gel Extraction kit using the manufacturer's protocol.

The ligation reaction was performed overnight at 16 °C in a 1.5 ml tube. The reaction mixture is vortexed and spun down right before the addition of the ligase enzyme, and once the enzyme is added, it's mixed by gently tapping, followed by a short spin, and then incubated at 16 °C.

	Nup205 sh1/sh3	Cut vector Control	Uncut vector control
Vector (Cut Vector: 26 ng/µl, Uncut vector: 4.5 µg/µl)	1.5 µl	1.5 µl	0.2 µl
Annealed Insert	1.0 µl	-	-
10x Ligation Buffer	1.0 µl	1.0 µl	1.0 µl
T4 DNA Ligase	1.0 µl	1.0 µl	-
NFW	5.5 µl	6.5 µl	9 µl
Total	10 µl	10 µl	10.2 µl

The ligated products are transformed into competent DH5α cells. DH5α cells were taken out on ice and when they thaw, the entire ligation reaction contents are added into it. This is incubated on ice for 20-30 mins. It is then given a 45 second heat shock at 42 °C. It is then immediately transferred onto ice for 10 mins. 250 µl of LB is added to the cells and incubated while shaking for 1 hour at 37 °C. These are then plated on LB Agar plates containing 100 µg/ml Ampicillin and incubated at 37 °C overnight (~16-18 hrs). Four individual colonies were picked from the two shRNA plasmids and were grown as primary culture in 1 ml LB (with 100 µg/ml Ampicillin) with shaking at 37 °C for 7-8 hours (until turbid). The entire primary culture is then used to prepare secondary culture in 10 ml LB (with 100 µg/ml Ampicillin) overnight at 37 °C, with shaking. The culture is spun down at 4000 RPM for 25 mins to pellet down the cells. From this pellet, the plasmid is isolated using Gene-all Exprep Plasmid SV mini kit according to the manufacturer's protocol. The final plasmid is resuspended in 30 µl NFW.

The insertion of the shRNA sequence is validated using XhoI digestion. Digestion is performed at 37 °C for ~3-4 hrs. The reaction mixture is then run on 2% agarose gel at 120 V and the bands around 100-200 bp are noted.

	DIgestion Reaction
Plasmid DNA (7 µg/µl)	1 µl
XhoI	1 µl
10x CutSmart	3 µl
NFW	25 µl
Total	30 µl

Reagents used in cloning: NEBuffer 3 (New England Biolabs, #B7003S), CutSmart (New England Biolabs, #B7204S), QIAquick Gel Extraction kit (QIAGEN, Cat No./ID: 28704), AgeI Hf (New England Biolabs, #R3552S), EcoRI Hf (New England Biolabs, #R3101S), T4 DNA Ligase (New England Biolabs, #M0202S), 10x T4 DNA Ligase Reaction Buffer (New England Biolabs, #B0202S), Exprep Plasmid SV mini (Gene-all, Cat. 101-150), XhoI (New England Biolabs, #R0146S)

Image Analysis

Analysis of cell area from were performed in the Fiji distribution of ImageJ. Cell areas were marked out using the freehand tool and areas were measured using the Analyse>Measure option. Project student Somdatta Majumdar helped perform the analysis done in (Fig. 10).

In-silico data analysis

ChIP-Seq analysis was performed using WashU Epigenome Browser. The publically available ChIP-Seq tracks used were: SMC3 - human, neural cell; CTCF - human, neural cell; Rad21 - human, neural cell; YY1 - human, H1-hESC and NT2/D1; MYC - human, A549 and H1-hESC; ZNF143 - human, H1-hESC.

Colocalization analysis was performed using the ‘Colocalization’ tool from ChIP-Atlas.

APPENDIX

Sequencing results for Nup205shRNA

1. Nup205 sh1

..CCCCCTCCACCCCGAGGGGACCCGACAGGCCCGAAGGAATAGAAGAAGAAG
GTGGAGAGAGAGACAGAGACAGATCCATTCGATTAGTGAACGGATCTCGACGG
TATCGATCACGAGACTAGCCTCGAGCGGCCGCAATATTTGCATGTCGCTATGTG
TTCTGGGAAATCACCATAAACGTGAAATCCCTATCAGTGATAGAGACTTATAAGT
TCCCTATCAGTGATAGAGACA**CCGGAGATGGTGAAGGAGGAATATTCTCGAGA**
ATATTCCTCCTCACCATCTTTTTTAATTCTCGACCTCGAGACAAATGGCAGTATT
CATCCACAATTTTAAAAGAAAAGGGGGGATTGGGGGGTACAGTGCAGGGGAAA
GAATAGTAGACATAATAGCAACAGACATACAAACTAAAGAATTACAAAAACAAAT
TACAAAAATTCAAAATTTTCGGGTTTATTACAGGGACAGCAGAGATCCACTTTGG
CCGCGGCTCGAGGGGGTTGGGGTTGCGCCTTTTCCAAGGCAGCCCTGGGTTT
GCGCAGGGACGCGGCTGCTCTGGGCGTGGTTCCGGGAAACGCAGCGGCGCC
GACCCTGGGTCTCGCACATTCTTCACGTCCGTTCGCAGCGTCACCCGGATCTT
CGCCGCTACCCTTGTGGGCCCCCCGGCGACGCTTCCTGCTCCGCCCCTAAGT
CGGGAAGGTTCCTTGCGGTTCGCGGCGTGCCGGACGTGACAAACGGAAGCCG
CACGTCTCACTAGTACCCTCGCAGACGGACAGCGCCAGGGAGCAATGGCAGC
GCGCCGACCGCGATGGGCTGTGGCCAATAGCGGCTGCTCAGCAGGGCGCGC
CGAGAGCAGCGGCCGGGAAGGGGCGGTGCGGGAGGCGGGGTGTGGGGCGG
TAGTGTGGGCCCTGTTCCTGCCCGCGCGGTGTTCCGCATTCTGCAAGCCTCCG
GAGCGCACGTCGGCAGTCGGCTCCCTCGTTGACCGAATCACCGACCTCTCTCC
CCAGGGGGATCTGTGAGTTTGGGGACCCTTGATTGTTCTTTCTTTTTCGCTATT
GTAAAATTCATGTTATATGGAGGGGGCAAAGTTTTCAGGGTGTTGTTTAGAATG
GGAAGATGTCCCTTGTATCACCATGGACCCTCATGATAATTTTGTTTCTTTCACT
TTCTACTCTGTTGACAACCATTGTCTCCTCTTATTTTCTTTTCATTTTCGGGAACT
TTTTCGTTAAACTTTAGCTTGCATTTTGAACAAATTTTTAAATTC..

2. Nup205 sh3

..CCCCCTCCACCCCGAGGGGACCCGACAGGCCCGAAGGAATAGAAGAAGAAG

GTGGAGAGAGAGACAGAGACAGATCCATTCGATTAGTGAACGGATCTCGACGG
TATCGATCACGAGACTAGCCTCGAGCGGCCGCAATATTTGCATGTCGCTATGTG
TTCTGGGAAATCACCATAAACGTGAAATCCCTATCAGTGATAGAGACTTATAAGT
TCCCTATCAGTGATAGAGACA**CCGGGCCAGTGCTTAGGACTACTAACTCGAGT**
TAGTAGTCCTAAGCACTGGCTTTTTAATTCTCGACCTCGAGACAAATGGCAGTA
TTCATCCACAATTTTAAAAGAAAAGGGGGGATTGGGGGGTACAGTGCAGGGGA
AAGAATAGTAGACATAATAGCAACAGACATACAAACTAAAGAATTACAAAGACAA
ATTACAAAAATTCAAAATTTTCGGGTTTATTACAGGGACAGCAGAGATCCACTTT
GGCCGCGGCTCGAGGGGGTTGGGGTTGCGCCTTTTCCAAGGCAGCCCTGGGT
TTGCGCAGGGACGCGGCTGCTCTGGGCGTGGTTCCGGGAAACGCAGCGGCGC
CGACCCTGGGTCTCGCACATTCTTCACGTCCGTTCGCAGCGTCACCCGGATCT
TCGCCGCTACCCTTGTGGGCCCCCCGGCGACGCTTCCTGCTCCGCCCCTAAGT
CGGGAAGGTTCCTTGCGGTTCGCGGCGTGCCGGACGTGACAAACGGAAGCCG
CACGTCTCACTAGTACCCTCGCAGACGGACAGCGCCAGGGAGCAATGGCAGC
GCGCCGACCGCGATGGGCTGTGGCCAATAGCGGCTGCTCAGCAGGGCGCGC
CGAGAGCAGCGGCCGGGAAGGGGCGGTGCGGGAAGCGGGGTGTGGGGCGG
TAGTGTGGGCCCTGTTCCTGCCCGCGCGGTGTTCCGCATTCTGCAAGCCTCCG
GAGCGCACGTCGGCAGTCGGCTCCCTCGTTGACCGAATCACCGACCTCTCTCC
CAGGGGGATCTGTGAGTTTGGGGACCCTTGATTGTTCATTCTTTNTCCCTATTG
TAAAATCATGTTATATGGACGGGCAAAGTTTTCAGGGTGTTGTTTAAAATGGGAA
GATGTCCCTTGAATACCATGGACCNNTGAAAATTTGGT..

Letters in bold represent the sequence of the insert.

REFERENCES

Andrews, P.W. (1984). Retinoic acid induces neuronal differentiation of a cloned human embryonal carcinoma cell line in vitro. Dev. Biol. *103*, 285–293.

Andrews, P.W., Damjanov, I., Berends, J., Kumpf, S., Zappavigna, V., Mavilio, F., and Sampath, K. (1994). Inhibition of proliferation and induction of differentiation of pluripotent human embryonal carcinoma cells by osteogenic protein-1 (or bone morphogenetic protein-7). Lab. Invest. *71*, 243–251.

Artavanis-Tsakonas, S., Rand, M.D., and Lake, R.J. (1999). Notch signaling: cell fate control and signal integration in development. Science *284*, 770–776.

Bailey, S.D., Zhang, X., Desai, K., Aid, M., Corradin, O., Cowper-Sal Lari, R., Akhtar-Zaidi, B., Scacheri, P.C., Haibe-Kains, B., and Lupien, M. (2015). ZNF143 provides sequence specificity to secure chromatin interactions at gene promoters. Nat. Commun. *2*, 6186.

Beagan, J.A., Duong, M.T., Titus, K.R., Zhou, L., Cao, Z., Ma, J., Lachanski, C.V., Gillis, D.R., and Phillips-Cremins, J.E. (2017). YY1 and CTCF orchestrate a 3D chromatin looping switch during early neural lineage commitment. Genome Res. *27*, 1139–1152.

Bestembayeva, A., Kramer, A., Labokha, A.A., Osmanović, D., Liashkovich, I., Orlova, E.V., Ford, I.J., Charras, G., Fassati, A., and Hoogenboom, B.W. (2015). Nanoscale stiffness topography reveals structure and mechanics of the transport barrier in intact nuclear pore complexes. Nat. Nanotechnol. *10*, 60–64.

Boncinelli, E., Simeone, A., Acampora, D., and Mavilio, F. (1991). HOX gene activation by retinoic acid. Trends Genet. *7*, 329–334.

Bowles, K.R., Tcw, J., Qian, L., Jadow, B.M., and Goate, A.M. (2019). Reduced variability of neural progenitor cells and improved purity of neuronal cultures using magnetic activated cell sorting. PLoS ONE *14*, e0213374.

Buchwalter, A.L., Liang, Y., and Hetzer, M.W. (2014). Nup50 is required for cell differentiation and exhibits transcription-dependent dynamics. Mol. Biol. Cell *25*,

2472–2484.

Capelson, M., Liang, Y., Schulte, R., Mair, W., Wagner, U., and Hetzer, M.W. (2010). Chromatin-bound nuclear pore components regulate gene expression in higher eukaryotes. Cell *140*, 372–383.

Caricasole, A., Ward-van Oostwaard, D., Zeinstra, L., van den Eijnden-van Raaij, A., and Mummery, C. (2000). Bone morphogenetic proteins (BMPs) induce epithelial differentiation of NT2D1 human embryonal carcinoma cells. Int. J. Dev. Biol. *44*, 443–450.

Casolari, J.M., Brown, C.R., Komili, S., West, J., Hieronymus, H., and Silver, P.A. (2004). Genome-wide localization of the nuclear transport machinery couples transcriptional status and nuclear organization. Cell *117*, 427–439.

Constantinescu, D., Gray, H.L., Sammak, P.J., Schatten, G.P., and Csoka, A.B. (2006). Lamin A/C expression is a marker of mouse and human embryonic stem cell differentiation. Stem Cells *24*, 177–185.

Coyle, D.E., Li, J., and Baccei, M. (2011). Regional differentiation of retinoic acid-induced human pluripotent embryonic carcinoma stem cell neurons. PLoS ONE *6*, e16174.

Dressler, G.R., and Gruss, P. (1989). Anterior boundaries of Hox gene expression in mesoderm-derived structures correlate with the linear gene order along the chromosome. Differentiation. *41*, 193–201.

Duboule, D. (2007). The rise and fall of Hox gene clusters. Development *134*, 2549–2560.

D'Angelo, M.A., Gomez-Cavazos, J.S., Mei, A., Lackner, D.H., and Hetzer, M.W. (2012). A change in nuclear pore complex composition regulates cell differentiation. Dev. Cell *22*, 446–458.

Ellis, P., Fagan, B.M., Magness, S.T., Hutton, S., Taranova, O., Hayashi, S., McMahon, A., Rao, M., and Pevny, L. (2004). SOX2, a persistent marker for multipotential neural stem cells derived from embryonic stem cells, the embryo or the adult. Dev. Neurosci. *26*, 148–165.

Engler, A.J., Sen, S., Sweeney, H.L., and Discher, D.E. (2006). Matrix elasticity directs stem cell lineage specification. Cell *126*, 677–689.

Ferri, A.L.M., Cavallaro, M., Braida, D., Di Cristofano, A., Canta, A., Vezzani, A., Ottolenghi, S., Pandolfi, P.P., Sala, M., DeBiasi, S., et al. (2004). Sox2 deficiency causes neurodegeneration and impaired neurogenesis in the adult mouse brain. Development *131*, 3805–3819.

Gokhale, P.J., Giesberts, A.M., and Andrews, P.W. (2000). Brachyury is expressed by human teratocarcinoma cells in the absence of mesodermal differentiation. Cell Growth Differ. *11*, 157–162.

Grandbarbe, L., Bouissac, J., Rand, M., Hrabé de Angelis, M., Artavanis-Tsakonas, S., and Mohier, E. (2003). Delta-Notch signaling controls the generation of neurons/glia from neural stem cells in a stepwise process. Development *130*, 1391–1402.

Griffis, E.R., Altan, N., Lippincott-Schwartz, J., and Powers, M.A. (2002). Nup98 is a mobile nucleoporin with transcription-dependent dynamics. Mol. Biol. Cell *13*, 1282–1297.

Heins, N., Malatesta, P., Cecconi, F., Nakafuku, M., Tucker, K.L., Hack, M.A., Chapouton, P., Barde, Y.-A., and Götz, M. (2002). Glial cells generate neurons: the role of the transcription factor Pax6. Nat. Neurosci. *5*, 308–315.

Ibarra, A., Benner, C., Tyagi, S., Cool, J., and Hetzer, M.W. (2016). Nucleoporin-mediated regulation of cell identity genes. Genes Dev. *30*, 2253–2258.

Kam, R.K.T., Deng, Y., Chen, Y., and Zhao, H. (2012). Retinoic acid synthesis and functions in early embryonic development. Cell Biosci. *2*, 11.

Kang, S., Chen, X., Gong, S., Yu, P., Yau, S., Su, Z., Zhou, L., Yu, J., Pan, G., and Shi, L. (2017). Characteristic analyses of a neural differentiation model from iPSC-derived neuron according to morphology, physiology, and global gene expression pattern. Sci. Rep. *7*, 12233.

Labade, A.S., Karmodiya, K., and Sengupta, K. (2016). HOXA repression is mediated by nucleoporin Nup93 assisted by its interactors Nup188 and Nup205.

Epigenetics Chromatin *9*, 54.

Labade, A.S., Salvi, A., Karmodiya, K., and Sengupta, K. (2019). Nup93 modulates spatiotemporal dynamics and function of the HOXA gene cluster during differentiation. BioRxiv.

Ladiwala, U., Basu, H., and Mathur, D. (2012). Assembling neurospheres: dynamics of neural progenitor/stem cell aggregation probed using an optical trap. PLoS ONE *7*, e38613.

Mahajani, S., Giacomini, C., Marinaro, F., De Pietri Tonelli, D., Contestabile, A., and Gasparini, L. (2017). Lamin B1 levels modulate differentiation into neurons during embryonic corticogenesis. Sci. Rep. *7*, 4897.

Nagai, S., Dubrana, K., Tsai-Pflugfelder, M., Davidson, M.B., Roberts, T.M., Brown, G.W., Varela, E., Hediger, F., Gasser, S.M., and Krogan, N.J. (2008). Functional targeting of DNA damage to a nuclear pore-associated SUMO-dependent ubiquitin ligase. Science *322*, 597–602.

Nagao, M., Sugimori, M., and Nakafuku, M. (2007). Cross talk between notch and growth factor/cytokine signaling pathways in neural stem cells. Mol. Cell. Biol. *27*, 3982–3994.

Nelson, P.T., Kondziolka, D., Wechsler, L., Goldstein, S., Gebel, J., DeCesare, S., Elder, E.M., Zhang, P.J., Jacobs, A., McGrogan, M., et al. (2002). Clonal human (hNT) neuron grafts for stroke therapy: neuropathology in a patient 27 months after implantation. Am. J. Pathol. *160*, 1201–1206.

Okumura, K., Nakamachi, K., Hosoe, Y., and Nakajima, N. (2000). Identification of a novel retinoic acid-responsive element within the lamin A/C promoter. Biochem. Biophys. Res. Commun. *269*, 197–202.

Phillips-Cremins, J.E., Sauria, M.E.G., Sanyal, A., Gerasimova, T.I., Lajoie, B.R., Bell, J.S.K., Ong, C.-T., Hookway, T.A., Guo, C., Sun, Y., et al. (2013). Architectural protein subclasses shape 3D organization of genomes during lineage commitment. Cell *153*, 1281–1295.

Pierce, T., Worman, H.J., and Holy, J. (1999). Neuronal differentiation of NT2/D1

teratocarcinoma cells is accompanied by a loss of lamin A/C expression and an increase in lamin B1 expression. Exp. Neurol. *157*, 241–250.

Przyborski, S.A., Christie, V.B., Hayman, M.W., Stewart, R., and Horrocks, G.M. (2004). Human embryonal carcinoma stem cells: models of embryonic development in humans. Stem Cells Dev. *13*, 400–408.

Ribes, V., Stutzmann, F., Bianchetti, L., Guillemot, F., Dollé, P., and Le Roux, I. (2008). Combinatorial signalling controls Neurogenin2 expression at the onset of spinal neurogenesis. Dev. Biol. *321*, 470–481.

Sasaki, N., Kiso, M., Kitagawa, M., and Saga, Y. (2011). The repression of Notch signaling occurs via the destabilization of mastermind-like 1 by Mesp2 and is essential for somitogenesis. Development *138*, 55–64.

Schermelleh, L., Carlton, P.M., Haase, S., Shao, L., Winoto, L., Kner, P., Burke, B., Cardoso, M.C., Agard, D.A., Gustafsson, M.G.L., et al. (2008). Subdiffraction multicolor imaging of the nuclear periphery with 3D structured illumination microscopy. Science *320*, 1332–1336.

Simões, P.D., and Ramos, T. (2007). Human pluripotent embryonal carcinoma NTERA2 cl.D1 cells maintain their typical morphology in an angiomyogenic medium. J. Negat. Results Biomed. *6*, 5.

Skotheim, R.I., Lind, G.E., Monni, O., Nesland, J.M., Abeler, V.M., Fosså, S.D., Duale, N., Brunborg, G., Kallioniemi, O., Andrews, P.W., et al. (2005). Differentiation of human embryonal carcinomas in vitro and in vivo reveals expression profiles relevant to normal development. Cancer Res. *65*, 5588–5598.

Solovei, I., Wang, A.S., Thanisch, K., Schmidt, C.S., Krebs, S., Zwerger, M., Cohen, T.V., Devys, D., Foisner, R., Peichl, L., et al. (2013). LBR and lamin A/C sequentially tether peripheral heterochromatin and inversely regulate differentiation. Cell *152*, 584–598.

Swift, J., Ivanovska, I.L., Buxboim, A., Harada, T., Dingal, P.C.D.P., Pinter, J., Pajerowski, J.D., Spinler, K.R., Shin, J.-W., Tewari, M., et al. (2013). Nuclear lamin-A scales with tissue stiffness and enhances matrix-directed differentiation. Science

341, 1240104.

Takamori, Y., Hirahara, Y., Wakabayashi, T., Mori, T., Koike, T., Kataoka, Y., Tamura, Y., Kurebayashi, S., Kurokawa, K., and Yamada, H. (2018). Differential expression of nuclear lamin subtypes in the neural cells of the adult rat cerebral cortex. IBRO Rep. *5*, 99–109.

Takemoto, T., Uchikawa, M., Yoshida, M., Bell, D.M., Lovell-Badge, R., Papaioannou, V.E., and Kondoh, H. (2011). Tbx6-dependent Sox2 regulation determines neural or mesodermal fate in axial stem cells. Nature *470*, 394–398.

Taylor, H.S. (2000). The role of HOX genes in the development and function of the female reproductive tract. Semin. Reprod. Med. *18*, 81–89.

Tsai, Y.-T., Itokazu, Y., and Yu, R.K. (2016). GM1 ganglioside is involved in epigenetic activation loci of neuronal cells. Neurochem. Res. *41*, 107–115.

Xu, M., Zhao, G.-N., Lv, X., Liu, G., Wang, L.Y., Hao, D.-L., Wang, J., Liu, D.-P., and Liang, C.-C. (2014). CTCF controls HOXA cluster silencing and mediates PRC2-repressive higher-order chromatin structure in NT2/D1 cells. Mol. Cell. Biol. *34*, 3867–3879.

Yang, E., Liu, N., Tang, Y., Hu, Y., Zhang, P., Pan, C., Dong, S., Zhang, Y., and Tang, Z. (2015). Generation of neurospheres from human adipose-derived stem cells. Biomed Res. Int. *2015*, 743714.

Yasuhiko, Y., Haraguchi, S., Kitajima, S., Takahashi, Y., Kanno, J., and Saga, Y. (2006). Tbx6-mediated Notch signaling controls somite-specific Mesp2 expression. Proc Natl Acad Sci USA *103*, 3651–3656.

Yeung, T., Georges, P.C., Flanagan, L.A., Marg, B., Ortiz, M., Funaki, M., Zahir, N., Ming, W., Weaver, V., and Janmey, P.A. (2005). Effects of substrate stiffness on cell morphology, cytoskeletal structure, and adhesion. Cell Motil. Cytoskeleton *60*, 24–34.

Zinin, N., Adameyko, I., Wilhelm, M., Fritz, N., Uhlén, P., Ernfors, P., and Henriksson, M.A. (2014). MYC proteins promote neuronal differentiation by controlling the mode of progenitor cell division. EMBO Rep. *15*, 383–391.

Zuo, B., Yang, J., Wang, F., Wang, L., Yin, Y., Dan, J., Liu, N., and Liu, L. (2012). Influences of lamin A levels on induction of pluripotent stem cells. Biol. Open *1*, 1118–1127.